Multiterminal ballistic Josephson junctions coupled to normal leads

Régis Mélin
Univ. Grenoble-Alpes, CNRS, Grenoble INP, Institut NEEL, 38000 Grenoble, France

(Received 19 October 2021; revised 3 January 2022; accepted 19 April 2022; published 27 April 2022)

Multiterminal Josephson junctions have aroused considerable theoretical interest recently and numerous works aim at putting the predictions of correlations among Coopers (i.e., the so-called quartets) and simulation of topological matter to the test of experiments. This paper is motivated by recent experimental investigation from the Harvard group reporting $h/4e$-periodic quartet signal in a four-terminal configuration containing a loop pierced by magnetic flux, together with inversion controlled by the bias voltage, i.e., the quartet signal can be larger at half-flux quantum than in zero magnetic field. Here, we theoretically focus on devices consisting of finite-size quantum dots connected to four superconducting leads and to a normal lead. In addition to presenting numerical calculations of the quartet signal within a simplified modeling, we reduce the device to a non-Hermitian Hamiltonian in the infinite-gap limit. Then, relaxation has the surprising effect of producing sharp peaks and log-normal variations in the voltage sensitivity of the quartet signal in spite of the expected moderate fluctuations in the two-terminal DC Josephson current. The phenomenon is reminiscent of a resonantly driven harmonic oscillator having amplitude inverse proportional to the damping rate, and of the thermal noise of a superconducting weak link, inverse proportional to the Dynes parameter. Perspectives involve quantum bath engineering multiterminal Josephson junctions in the circuits of cavity quantum electrodynamics.

DOI: 10.1103/PhysRevB.105.155418

I. INTRODUCTION

BCS superconductors [1] are characterized by macroscopic phase variable φ and energy gap Δ between the ground state and the first quasiparticles. Anderson demonstrated [2,3] that the interplay between Coulomb interaction and collective modes in bulk superconductors yields the Higgs mechanism as an explanation to the Meissner effect. Josephson [4] demonstrated that gauge invariance implies DC supercurrent between two phase-biased superconductors, and AC current oscillations with voltage biasing. The so-called Andreev bound states (ABS) [5–8] contribute to the DC Josephson supercurrent flowing through any type of weak link (see, for instance, Refs. [9–13]). Recently, the ABS were probed with microwave spectroscopy [14–17], but the lifetime of this "Andreev qubit" [18] turns out not to be infinite. In general, understanding the mechanisms of quasiparticle poisoning [19–26] is a central issue in the studies of circuits of quantum engineering [27–31]. In bulk superconductors, the electron-phonon coupling or the electron-electron repulsive Coulomb interaction produce finite quasiparticle lifetime [32–35] captured by adding a small imaginary part η to their energy. This small Dynes parameter η [32–35] produces exponential time decay of the quasiparticle wave functions. In this paper, we investigate multiterminal Josephson junctions coupled to normal leads, and demonstrate that small relaxation produced by the coupling to those normal conductors has a drastic effect on the current. Based on previous works related to infinite-gap Hamiltonians [18,36,37], we also here consider the infinite-gap limit, where non-Hermitian Hamiltonians emerge for quantum dots coupled to superconducting and normal leads. Those non-Hermitian Hamiltonians receive interpretation of describing the coherent oscillations and damping in the ABS dynamics, and they capture the degrees of freedom of the ABS having spatial extent set by the BCS coherence length, which is vanishingly small in the infinite-gap limit. This paper also suggests the interest of future quantum bath engineering for multiterminal Josephson junctions connected to cavity-quantum electrodynamics resonators.

Now, we specifically introduce the considered four-terminal Josephson junctions, starting with the three-terminal Cooper pair beam splitters that have been the subject of intense investigations for more than 20 years. Entangled Andreev pairs can split if two independent voltages are applied in three-terminal F_aSF_b ferromagnet-superconductor-ferromagnet or N_aSN_b normal-metal–superconductor–normal-metal Cooper pair beam splitters [38–65]. "Nonlocal" or "crossed" Andreev reflection (CAR) appears if the separation between the N_aS and SN_b interfaces is comparable to the zero-energy superconducting coherence length. Spin-up electron from lead N_b can be Andreev reflected as spin-down hole into N_a, leaving a Cooper pair in the "central" S. This yields nonlocal current response reflecting production of nonlocally split Cooper pairs. In addition, the positive current-current cross correlations of Cooper pair splitting [40,66–77] were experimentally revealed [59,60].

The double quantum dot experiments [57,58,60] provide evidence for nonlocal two-particle Andreev resonance in N_a-dot-S_c-dot-N_b devices, on the condition of the opposite energy levels $\varepsilon_a = -\varepsilon_b$ on both quantum dots. In the following, we demonstrate how "nonlocal two-particle Andreev

resonance" in N_a-dot-S_c-dot-N_b Cooper pair beam splitters can be generalized to "nonlocal two-Cooper-pair resonance" in all-superconducting three-terminal Josephson junctions.

Those two-Cooper-pair resonances build on nonlocal two-Cooper-pair states, the so-called quartets [78–92] that appear in (S_a, S_c, S_b) three-terminal Josephson junctions, where S_a and S_b are voltage-biased at V_a and V_b, the superconducting lead S_c being grounded at $V_c = 0$. Andreev scattering yields quartet phase-sensitive DC current response if the condition $V_a = -V_b \equiv V$ is fulfilled. On this quartet line $V_a = -V_b$, the elementary transport process transfers two Cooper pairs from S_a and S_b into the grounded S_c, while exchanging partners [78–92]. By the time-energy uncertainty relation, this phase-sensitive quartet current is DC since, on the quartet line, the energy $E_i = 2e(V_a + V_b)$ of two Cooper pairs from S_a and S_b in the initial state is equal to the final-state energy $E_f = 4eV_c$ of the two Cooper pairs transmitted into S_c.

Several experiments were recently performed on multiterminal Josephson junctions [93–104]. Some of those explored the possibility of nontrivial topology [37,92,94,105–120]. On the other hand, three groups reported compatibility with the quartets [78–92]: the Grenoble group experiment with metallic structures [93], the Weizmann Institute group experiment with semiconducting nanowires [95], and the more recent Harvard group experiment on ballistic graphene-based four-terminal Josephson junctions [97]. This third experiment [97] is summarized in Figs. 1(a) and 1(b). The latter shows typical experimental variations for the quartet critical current as a function of the bias voltage V and the magnetic flux Φ through the loop. The experiment features the counterintuitive voltage-V-tunable inversion, i.e., the possibility of stronger quartet critical current at half-flux quantum $\Phi = \pi$ than in zero field $\Phi = 0$ [see Fig. 1(b)]. This paper is motivated by exploring interpretation of this experiment, in the continuation of our previous papers I and II [87,88]. We also underline two recent experimental preprints reporting the quartet line in ballistic devices [103,104].

Zero-dimensional (0D) quantum dots were used in Ref. [121] to model two-terminal graphene-superconductor hybrids, in connection with experimental evidence for the Floquet replica of the Andreev spectrum under microwave radiation. The goal of this paper is to similarly describe four-terminal graphene-based Josephson junctions with effective models based on quantum dots, in the absence of Coulomb interaction. We argue that multilevel quantum dots coupled to four superconducting leads and to a normal lead are "minimal models" of four-terminal Josephson junctions that are intermediate between the short- and long-junction limits. In addition, we further simplify the description in terms of double 0D quantum dots. Four or more ABS are within the gap in the equilibrium limit, instead of two ABS for a single 0D quantum dot.

Importantly, nonproximitized regions can appear in the two-dimensional (2D) metal, typically in the "crosslike region" formed in-between the contacts with the superconductors [see Fig. 1(a)]. Then, the quantum transport process can have initial or final states in those normal regions of the circuit. Current lines can be converted by Andreev reflection as supercurrent flowing in the grounded superconducting loop. Namely, current conservation for symmetric coupling to the superconducting leads implies that the 2D metal chemical potential is at the same zero energy as in the superconducting loop. Thus, the normal carriers transmitted through the 2D metal can be transferred into the grounded superconducting loop without taking or giving energy.

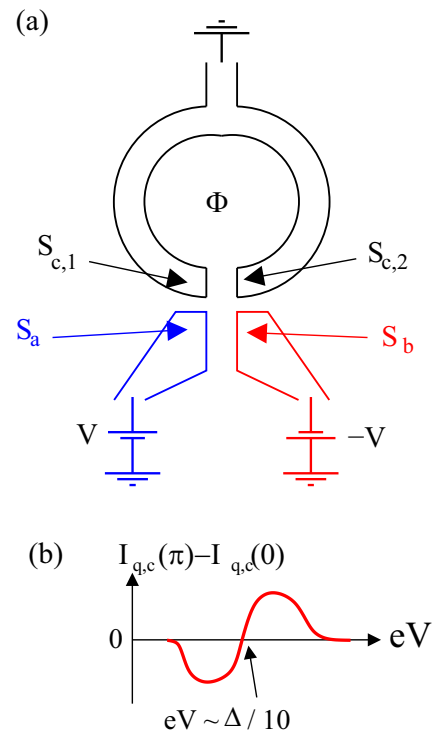

FIG. 1. Schematic four-terminal experiment. (a) Represents top view of the experimental device, with the superconducting leads S_a and S_b biased at $V_{a,b} = \pm V$. The loop terminated by $S_{c,1}$ and $S_{c,2}$ is connected to ground by the contact on top of it, and it is pierced by the magnetic field flux Φ. The four superconducting leads are evaporated on a graphene layer gated far from the Dirac point, and form a two-dimensional (2D) metal. (b) Summarizes the experimental result [97] that inspires the present theoretical paper, i.e., the quartet critical current current $I_{q,c}(\pi)$ at flux $\Phi = \pi$ can be larger or smaller than $I_{q,c}(0)$ at flux $\Phi = 0$, in a way that is sensitive to voltage typically being in the range $eV \approx \Delta/10$ where Δ is the superconducting gap.

Now, we explain the connection between this work and our previous papers. Compared to our previous Ref. [83], we implement a double 0D quantum dot instead of the single quantum dot Dynes parameter [32–35] model of Ref. [83]. We also include four superconducting leads, instead of three in our previous Ref. [83]. Our previous Paper I [87] presented an expansion of the quartet critical current in perturbation in the tunneling amplitudes between a 2D metal and four superconducting leads. This paper addresses resonances that appear beyond the weak coupling limit. Our previous Paper II [88] treated single quantum dot with relaxation solely originating from the continua of BCS quasiparticles. Relaxation then produces nonvanishingly small linewidth broadening δ_0 for the Floquet resonances, which behaves like $\log \delta_0 \sim -\Delta/eV$ at low-bias voltage energy eV compared to the superconducting gap Δ [83,84,88,116]. In the four-terminal device of Paper II [88], Landau-Zener quantum tunneling reduces the quartet current by coherent superpositions in the dynamics of the

two opposite current-carrying ABS, at voltage values that are close to avoided crossings in the Floquet spectra. This mechanism is analogous to the reduction of the DC Josephson current in microwave-irradiated weak links [122]. Conversely, in this work, the interplay between the time-periodic dynamics and finite linewidth broadening due to the attached normal lead restores the expected sharp resonance peaks in the voltage dependence of the quartet current. For instance, a resonantly driven harmonic oscillator has amplitude inverse proportional to the damping rate. In addition, we note that the zero-frequency noise of a single superconducting weak link at finite temperature is inverse proportional to the rate set by the Dynes parameter [32–35] in some parameter window (see Ref. [123]). The same scaling holds in this reference for the noise at frequency $2\omega_S$, where ω_S is the ABS energy. The quartets in four-terminal devices [87,88,97] offer several parameters to probe this physics, such as the quartet phase variable and the "knobs" of the bias voltage and magnetic flux.

The paper is organized as follows. The Hamiltonians are presented in Sec. II. The mechanism for the two-Cooper-pair resonance is discussed in Sec. III. The mechanism for the inversion is presented in Sec. IV. Section V shows numerical results. The low-voltage limit is discussed in Sec. VI. Concluding remarks are presented in the final Sec. VII.

II. HAMILTONIANS

In this section, we provide the Hamiltonians on which the paper is based. Section II A presents the full Hamiltonians of the superconductors, quantum dots, and normal leads. It goes beyond the goal of this paper to produce numerical results for the voltage-biased four-terminal Josephson junctions described by the general Hamiltonians of Sec. II A in a realistic geometry. This is why we present in Sec. II B simplified model Hamiltonians which will subsequently be used for numerical calculations.

A. General Hamiltonians

Now, we introduce in Sec. II A 1 the BCS Hamiltonian of the superconducting leads. Sections II A 2 and II A 3 introduce the Hamiltonians of the quantum dots and normal leads, respectively. As it is mentioned above, the numerical calculations presented below are based on simplifications of those Hamiltonians.

1. Superconductors

The Hamiltonian of a BCS superconductor is the following:

$$\mathscr{H}_{\rm BCS} = -W \sum_{\langle i,j\rangle} \sum_{\sigma_z=\uparrow,\downarrow} \left(c^+_{i,\sigma_z} c_{j,\sigma_z} + c^+_{j,\sigma_z} c_{i,\sigma_z}\right) - \Delta \sum_i \left(\exp(i\varphi_i) c^+_{i,\uparrow} c^+_{i,\downarrow} + \exp(-i\varphi_i) c_{i,\downarrow} c_{i,\uparrow}\right), \quad (1)$$

where $\sum_{\langle i,j\rangle}$ denotes summation over pairs of neighboring tight-binding sites labeled by i and j, and σ_z is the component of the spin along the quantization axis. The bulk hopping amplitude is denoted by W and the superconducting gap Δ is taken identical in all superconducting leads S_a, S_b, $S_{c,1}$, and $S_{c,2}$. The variable φ_i denotes the superconducting phase variable at the tight-binding site labeled by i. In the following, the current is weak and φ_i is approximated as being uniform in space, with the values φ_a, φ_b, $\varphi_{c,1}$, and $\varphi_{c,2}$ in S_a, S_b, $S_{c,1}$, and $S_{c,2}$, respectively.

We assume short distance between the contact points c_1 and c_2 (at the interfaces between $S_{c,1}$ or $S_{c,2}$ and the quantum dot), and we use the approximation of the gauge

$$\varphi_{c,1} = \varphi_c, \quad (2)$$

$$\varphi_{c,2} = \varphi_c + \Phi, \quad (3)$$

where Φ is the flux enclosed in the loop terminated by $S_{c,1}$ and $S_{c,2}$.

2. Double quantum dots

A legitimate approximation is to discard the Coulomb electron-electron repulsion at high transparency. Then the finite-size quantum dot is described by the Hamiltonian

$$\mathscr{H}_{\rm dot} = -W \sum_{\langle i,j\rangle} \sum_{\sigma_z=\uparrow,\downarrow} \left(c^+_{i,\sigma_z} c_{j,\sigma_z} + c^+_{j,\sigma_z} c_{i,\sigma_z}\right) \quad (4)$$

$$- \varepsilon_g \sum_i \sum_{\sigma_z=\uparrow,\downarrow} c^+_{i,\sigma_z} c_{i,\sigma_z}, \quad (5)$$

where the hopping amplitude W is identical to Eq. (1), and ε_g is proportional to the gate voltage. The summation over pairs of neighboring tight-binding sites is restricted to the region of finite dimension defining the quantum dot.

Conversely, the Hamiltonian of a single 0D quantum dot D_x at location $\mathbf{x}$ is the following:

$$\mathscr{H}_{D_x,0\rm D} = \varepsilon_x \sum_{\sigma_z} c^+_{D_x,\sigma_z} c_{D_x,\sigma_z}, \quad (6)$$

where ε_x is the onsite energy. Similarly, the double quantum dot (D_x, D_y) is characterized by the onsite energies ε_x and ε_y with tunneling amplitude $\Sigma^{(0)}$ between them:

$$\mathscr{H}_{D_y,0\rm D} = \varepsilon_y \sum_{\sigma_z} c^+_{D_y,\sigma_z} c_{D_y,\sigma_z}, \quad (7)$$

$$\mathscr{H}_{T,0} = -\Sigma^{(0)} \sum_{\sigma_z} c^+_{D_x,\sigma_z} c_{D_y,\sigma_z} + \text{H.c.} \quad (8)$$

At the exception of one of the numerical calculations presented in Sec. V, we use $\varepsilon_x = \varepsilon_y = 0$ in the paper, thus with

$$\mathscr{H}_{D_x,0\rm D} = 0, \quad (9)$$

$$\mathscr{H}_{D_y,0\rm D} = 0. \quad (10)$$

3. Normal leads

The Hamiltonian of a normal lead is given by

$$\mathscr{H}_N = -W \sum_{\langle i,j\rangle} \sum_{\sigma_z=\uparrow,\downarrow} \left(c^+_{i,\sigma_z} c_{j,\sigma_z} + c^+_{j,\sigma_z} c_{i,\sigma_z}\right),$$

where the normal-lead chemical potential is vanishingly small, and the hopping amplitude W is identical to Eq. (1). Equation (11) is similar to the quantum dot Hamiltonian given by Eq. (4) but, now, the summation over the pairs of neighboring tight-binding sites runs over an infinite lattice.

B. Simplified model Hamiltonians

Our previous Paper I [87] was based on perturbation theory in the tunnel amplitudes between a 2D metal and four superconducting leads, in the $V = 0^+$ adiabatic limit. In Paper I, the poles of the Green's functions are at the gap edge singularities and those perturbative calculations do not yield small voltage scales in the quartet critical current-voltage characteristics. In our previous Paper II, we addressed the connection between the quartet critical current and the Floquet spectra in a situation where 0D quantum dot is connected to four superconducting leads. We then obtained reduction of the quartet critical current at the bias-voltage resonance values. Compared to this Paper II, the here-considered four-terminal double quantum dot Josephson junction is additionally connected to a normal lead.

In this section, we provide the Hamiltonians of the three considered simplified models, the third one being numerically implemented in the forthcoming Sec. V. Section II B 1 deals with a multilevel quantum dot connected to four superconducting and to normal leads. Sections II B 2 and II B 3 deal with two simple models of double 0D quantum dots, also attached to superconducting and normal leads. Sections II B 2 and II B 3 correspond to "double 0D quantum dot connected to normal lead" in parallel or in series, respectively. The interest of double 0D quantum dots with respect to single, triple, or quadruple 0D quantum dots is explained in Sec. II B 4.

1. Multilevel quantum dot

Now, we consider the Hamiltonian of a multilevel quantum dot connected to superconducting and normal leads. We also provide a physical discussion. This defines a first stage in reducing the four-terminal device to simpler Hamiltonians.

We assume that the multilevel quantum dot on Fig. 2 is intermediate between the short- and long-junction limits, i.e., it has dimension $\gtrsim 2\xi_0$, where $\xi_0 = \hbar v_F/\Delta$ is the BCS coherence length, with v_F the Fermi velocity. Thus, more than two ABS are formed at equilibrium.

The Hamiltonian. We consider finite-size discrete levels on the multilevel quantum dot of Fig. 2, at the energies Ω_ψ. The corresponding Hamiltonian takes the form

$$\mathscr{H}_{\rm multi} = \sum_\psi \Omega_\psi \sum_{\sigma_z} c^+_{\psi,\sigma_z} c_{\psi,\sigma_z}, \tag{11}$$

where c^+_{ψ,σ_z} creates a fermion with spin σ_z in the state $|\psi\rangle$. The superconducting leads S_a, S_b, $S_{c,1}$, and $S_{c,2}$ are described by the BCS Hamiltonian given by Eq. (1). The normal lead is described by Eq. (11). Tunneling between the leads $(S_a, S_b, S_{c,1}, S_{c,2})$ biased at $(V, -V, 0, 0)$ and the multilevel quantum dot is described by multichannel contacts at the time τ:

$$\mathscr{H}_{T,a}(\tau) = -\Sigma_a^{(1)} \exp\left(-ieV\tau/\hbar\right) \sum_s \sum_{\sigma_z} c^+_{a_s,\sigma_z} c_{\alpha_s,\sigma_z} + \text{H.c.}, \tag{12}$$

$$\mathscr{H}_{T,b}(\tau) = -\Sigma_b^{(1)} \exp\left(ieV\tau/\hbar\right) \sum_t \sum_{\sigma_z} c^+_{b_t,\sigma_z} c_{\beta_t,\sigma_z} + \text{ H.c.}, \tag{13}$$

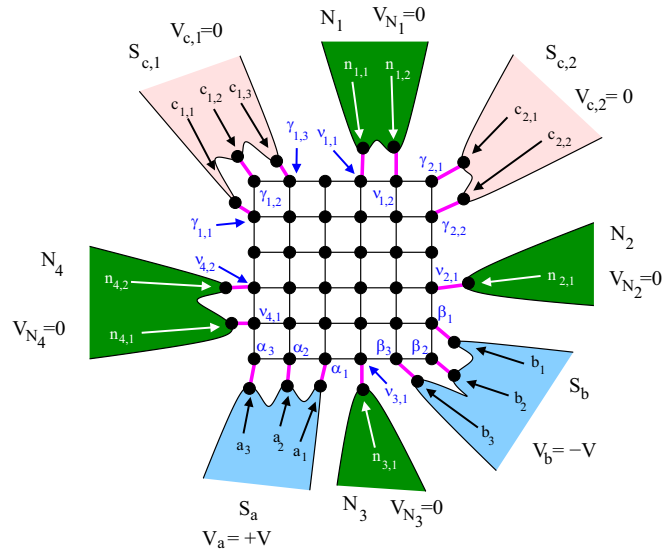

FIG. 2. The four-terminal superconducting multilevel quantum dot. The figure shows a multilevel quantum dot connected to the four superconducting leads S_a, S_b, $S_{c,1}$, and $S_{c,2}$ biased at $V_{a,b} = \pm V$ and $V_{c,1} = V_{c,2} = 0$, and to the four grounded normal leads N_1, N_2, N_3, and N_4. The tunneling between the multilevel quantum dot and the superconducting leads is provided in Eqs. (12)–(15). The tunneling to the normal leads is provided in Eq. (20). This model will be used in Secs. III A, III B 1, III B 2, III C, and III D.

$$\mathscr{H}_{T,c_1} = -\Sigma_{c_1}^{(1)} \sum_u \sum_{\sigma_z} c^+_{c_{1,u},\sigma_z} c_{\gamma_{1,u},\sigma_z} + \text{H.c.}, \tag{14}$$

$$\mathscr{H}_{T,c_2} = -\Sigma_{c_2}^{(1)} \sum_v \sum_{\sigma_z} c^+_{c_{2,v},\sigma_z} c_{\gamma_{2,v},\sigma_z} + \text{H.c.}, \tag{15}$$

where the integers s, t, u, and v label the collection of hopping amplitudes in real space, thus realizing a multichannel interface. As an approximation, the hopping amplitudes in Eqs. (12)–(15) were chosen identical within each contact: $\Sigma^{(1)}_{a,s} \equiv \Sigma^{(1)}_a$, $\Sigma^{(1)}_{b,t} \equiv \Sigma^{(1)}_b$, $\Sigma^{(1)}_{c_1,u} \equiv \Sigma^{(1)}_{c_1}$, and $\Sigma^{(1)}_{c_2,v} \equiv \Sigma^{(1)}_{c_2}$. The contact transparencies are parametrized by

$$\Gamma_a = \left(\Sigma_a^{(1)}\right)^2/W, \tag{16}$$

$$\Gamma_b = \left(\Sigma_b^{(1)}\right)^2/W, \tag{17}$$

$$\Gamma_{c_1} = \left(\Sigma_{c_1}^{(1)}\right)^2/W, \tag{18}$$

$$\Gamma_{c_2} = \left(\Sigma_{c_2}^{(1)}\right)^2/W. \tag{19}$$

The notations $c^+_{a_s,\sigma_z}$, $c^+_{b_t,\sigma_z}$, $c^+_{c_{1,u},\sigma_z}$, and $c^+_{c_{2,v},\sigma_z}$ refer to creating a spin-σ_z fermion at the tight-binding sites labeled by a_s, b_t, $c_{1,u}$, and $c_{2,v}$ belonging to the superconducting leads S_a, S_b, $S_{c,1}$, and $S_{c,2}$ [see (a_1, a_2, a_3), (b_1, b_2), $(c_{1,1}, c_{1,2}, c_{1,3})$, and $(c_{2,1}, c_{2,2})$ in Fig. 2]. Similarly, c_{α_s,σ_z}, c_{β_t,σ_z}, $c_{\gamma_{1,u},\sigma_z}$, and $c_{\gamma_{2,v},\sigma_z}$ destroy a spin-σ_z fermion at the tight-binding sites labeled by α_s, β_t, $\gamma_{1,u}$, and $\gamma_{2,v}$ [see $(\alpha_1, \alpha_2, \alpha_3)$, (β_1, β_2), $(\gamma_{1,1}, \gamma_{1,2}, \gamma_{1,3})$, and $(\gamma_{2,1}, \gamma_{2,2})$ in Fig. 2].

We assume in addition that q_0 normal leads labeled by $n_q = 1, \ldots, q_0$ are connected to the multilevel quantum dot by the

following tunneling Hamiltonian:

$$\mathscr{H}_{T,N_q} = -\Sigma^{(1)}_{N_q} \sum_{w} \sum_{\sigma_z} c^{+}_{n_{q,w},\sigma_z} c_{\nu_{q,w},\sigma_z} + \text{H.c.}, \tag{20}$$

where $n_{q,w}$ is the tight-binding site labeled by w in the lead N_q, and $\nu_{q,w}$ is its counterpart on the multilevel quantum dot. We took in Eq. (20) the same tunneling amplitudes $\Sigma^{(1)}_{N_q} \equiv \Sigma^{(1)}_{N_q,w}$ at each contact. For instance, for $q_0 = 4$, the tight-binding sites $(n_{1,1}, n_{1,2})$, $n_{2,1}$, $n_{3,1}$, and $(n_{4,1}, n_{4,2})$ belonging to the normal leads N_1, N_2, N_3, and N_4, respectively, are shown in Fig. 2, together with their counterparts $(\nu_{1,1}, \nu_{1,2})$, $\nu_{2,1}$, $\nu_{3,1}$, and $(\nu_{4,1}, \nu_{4,2})$ in the multilevel quantum dot.

This model will be used in the Secs. III A, III B 1, III B 2, III C, and III D.

Physical remarks. Two antagonist effects appear: (i) In absence of coupling to the superconductors, increasing the coupling to the normal leads has the tendency to smoothen the energy dependence of the local density of states. (ii) In the presence of coupling to the superconducting leads, the Floquet resonances produce sharp peaks in the local density of states as a function of energy.

Physically, the above item (i) captures the metallic limit of "weak sample-to-sample fluctuations in the quartet critical current." The item (ii) corresponds to "strong sample-to-sample fluctuations in the quartet current," where samples differ by the number of channels at the contacts, or by fluctuations in the shape of the multilevel quantum dot. The metallic limit (i) is ruled out for compatibility with the experiment in Ref. [97] because it does not produce small voltage scales. This is why we focus here on the regime (ii) of weak coupling to the normal leads.

In most of the work, we make an additional assumption about the spectrum $\{\Omega_\psi\}$ of the multilevel quantum dot [see Eq. (11)]. Namely, we assume pairs of levels at opposite energies, i.e., there are values ψ_1, ψ_2 of the label ψ such that $\Omega_{\psi_1} = -\Omega_{\psi_2}$. Then, two-Cooper-pair resonance emerges at specific values of the bias voltage, such as $2eV_* = \Omega_{\psi_1} - \Omega_{\psi_2} = 2\Omega_{\psi_1}$ in the limit of weak coupling. However, within the considered models, we will find in Sec. V robustness of the sharp resonances with respect to detuning from the condition of opposite energy levels.

Next, we simplify the multilevel quantum dot into phenomenological models of double 0D quantum dots that seem to be the "minimal models" for the two-Cooper-pair resonance.

2. Phenomenological model of double 0D quantum dot with normal lead in parallel

Now, we present the Hamiltonian of a double 0D quantum dot with normal lead in parallel, and additionally connected to superconducting leads. We also provide a physical discussion. This defines a second stage in proposing models that can practically be numerically implemented.

The Hamiltonian. Specifically, we consider a second model, i.e., a "phenomenological model of double 0D quantum dot with normal lead in parallel" (see Fig. 3). The quantum dots D_x and D_y have the vanishingly small Hamiltonians of Eqs. (9) and (10). The coupling between D_x and D_y is given by Eq. (8) with the hopping amplitude $\Sigma^{(0)}$ shown as a light blue line in Fig. 3. Again, the superconducting leads S_a, S_b, $S_{c,1}$, and $S_{c,2}$ are described by the BCS Hamiltonian [see Eq. (1)]. Tunneling between the leads S_a, S_b, $S_{c,1}$, and $S_{c,2}$ and the double 0D quantum dot (D_x, D_y) is described by single-channel contacts:

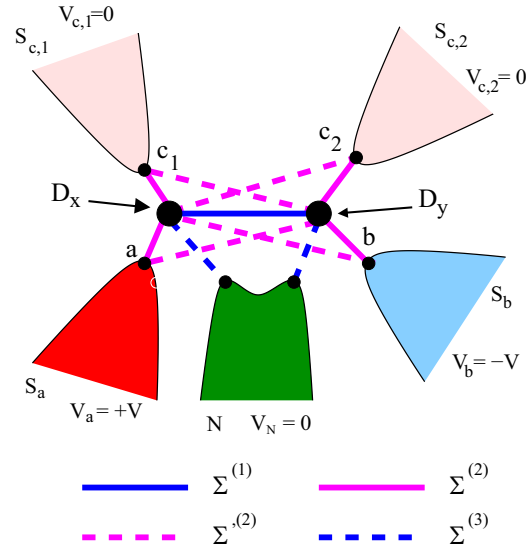

FIG. 3. The four-terminal phenomenological model of superconducting double 0D quantum dot with normal lead in parallel. The figure shows a double 0D quantum dot connected to the four superconducting leads S_a, S_b, $S_{c,1}$, and $S_{c,2}$ biased at $V_{a,b} = \pm V$ and $V_{c,1} = V_{c,2} = 0$, and to the four grounded normal leads N_1, N_2, N_3, and N_4. The corresponding Hamiltonian is provided in Sec. II B 2. The coupling $\Sigma^{(0)}$ directly couples the two quantum dots D_x and D_y [see Eq. (8)]. The "direct" coupling $\Sigma^{(2)}$ connects D_x to S_a, D_x to $S_{c,1}$, D_y to S_b, and D_y to $S_{c,2}$ [see Eqs. (21)–(25)]. The "crossed" coupling $\Sigma'^{(2)}$ connects D_x to S_b, D_x to $S_{c,2}$, D_y to S_a, and D_y to $S_{c,1}$ [see Eqs. (26)–(30)]. The coupling $\Sigma^{(3)}$ connects the 0D quantum dot D_x to N_x and D_y to N_y, where N_x and N_y are the two tight-binding sites on the normal-lead N side of the contacts [see Eqs. (31)–(33)]. This model will be used in Secs. III A, III B 1, III B 2, III B 3, III C, and III D.

$$\mathscr{H}_{T,D_x,a}(\tau) = -\Sigma^{(2)}_{D_x,a} \exp\left(-ieV\tau/\hbar\right) \sum_{\sigma_z} c^{+}_{a,\sigma_z} c_{D_x,\sigma_z} + \text{H.c.}, \tag{21}$$

$$\mathscr{H}_{T,D_y,b}(\tau) = -\Sigma^{(2)}_{D_y,b} \exp\left(ieV\tau/\hbar\right) \sum_{\sigma_z} c^{+}_{b,\sigma_z} c_{D_y,\sigma_z} + \text{H.c.}, \tag{22}$$

$$\mathscr{H}_{T,D_x,c_1} = -\Sigma^{(2)}_{D_x,c_1} \sum_{\sigma_z} c^{+}_{c_1,\sigma_z} c_{D_x,\sigma_z} + \text{H.c.}, \tag{23}$$

$$\mathscr{H}_{T,D_y,c_2} = -\Sigma^{(2)}_{D_y,c_2} \sum_{\sigma_z} c^{+}_{c_2,\sigma_z} c_{D_y,\sigma_z} + \text{H.c.}, \tag{24}$$

and we assume

$$\Sigma^{(2)}_{D_x,a} = \Sigma^{(2)}_{D_y,b} = \Sigma^{(2)}_{D_x,c_1} = \Sigma^{(2)}_{D_y,c_2} \equiv \Sigma^{(2)}. \tag{25}$$

We parametrize the contact transparency with $\Gamma = (\Sigma^{(2)})^2/W$.

In addition, we include the following "crossed tunneling terms" between D_x and S_b, $S_{c,2}$ and between D_y and S_a, $S_{c,1}$:

$$\mathscr{H}_{T,D_x,b}(\tau) = -\Sigma^{(2)}_{D_x,b} \exp(ieV\tau/\hbar) \sum_{\sigma_z} c^{+}_{b,\sigma_z} c_{D_x,\sigma_z} + \text{H.c.}, \tag{26}$$

$$\mathscr{H}_{T,D_y,a}(\tau) = -\Sigma^{(2)}_{D_y,a} \exp(-ieV\tau/\hbar) \sum_{\sigma_z} c^{+}_{a,\sigma_z} c_{D_y,\sigma_z} + \text{H.c.}, \tag{27}$$

$$\mathscr{H}_{T,D_x,c_2} = -\Sigma^{(2)}_{D_x,c_2} \sum_{\sigma_z} c^{+}_{c_2,\sigma_z} c_{D_x,\sigma_z} + \text{H.c.}, \tag{28}$$

$$\mathscr{H}_{T,D_y,c_1} = -\Sigma^{(2)}_{D_y,c_1} \sum_{\sigma_z} c^{+}_{c_1,\sigma_z} c_{D_y,\sigma_z} + \text{H.c.}, \tag{29}$$

and we assume

$$\Sigma^{(2)}_{D_x,b} = \Sigma^{(2)}_{D_y,a} = \Sigma^{(2)}_{D_x,c_2} = \Sigma^{(2)}_{D_y,c_1} \equiv \Sigma'^{(2)}. \tag{30}$$

We parametrize the crossed contact transparency with $\Gamma' = (\Sigma'^{(2)})^2/W$.

The Hamiltonian of the normal lead is given by Eq. (11). Tunneling between the quantum dots D_x, D_y and the normal lead N is realized with the single-channel contacts (D_x, N_x) and (D_y, N_y):

$$\mathscr{H}_{T,D_x,N_x} = -\Sigma^{(3)}_{D_x,N_x} \sum_{\sigma_z} c^{+}_{N_x,\sigma_z} c_{D_x,\sigma_z} + \text{H.c.}, \tag{31}$$

$$\mathscr{H}_{T,D_y,N_y} = -\Sigma^{(3)}_{D_y,N_y} \sum_{\sigma_z} c^{+}_{N_y,\sigma_z} c_{D_y,\sigma_z} + \text{H.c.}, \tag{32}$$

N_x and N_y being tight-binding sites belonging to the normal lead, and connected to D_x and D_y, respectively, by Eqs. (31) and (32). We additionally assume that $\Sigma^{(3)}_{D_x,N_x}$ and $\Sigma^{(3)}_{D_y,N_y}$ are identical:

$$\Sigma^{(3)}_{D_x,N_x} = \Sigma^{(3)}_{N_x,D_x} = \Sigma^{(3)}_{D_y,N_y} = \Sigma^{(3)}_{N_y,D_y} \equiv \Sigma^{(3)}. \tag{33}$$

This model will be used in Secs. III A, III B 1, III B 2, III B 3, III C, and III D.

Physical remarks. Once disconnected from the superconducting or normal leads, this phenomenological model of double 0D quantum dot with normal lead in parallel naturally yields the pair of opposite-energy levels that is relevant to the two-Cooper-pair resonance.

Now, we consider in Sec. II B 3 another phenomenological model that also includes the possibility of quartet current oscillating at the scale of the Fermi wavelength as a function a dimension of the device.

3. *Phenomenological model of double 0D quantum dot with normal lead in series*

Now, we consider the Hamiltonian of a double 0D quantum dot with normal lead in series, and connected to superconducting leads. We also provide a physical discussion. The numerical calculations presented in the forthcoming Sec. V are based on this third stage of the simplifications.

The Hamiltonian. Namely, we consider a third model, i.e., a "phenomenological model of double 0D quantum dot with normal lead in series" connected by single-channel contacts through a 2D metal (see Fig. 4). The difference with the previous Sec. II B 2 is in the coupling to the normal lead.

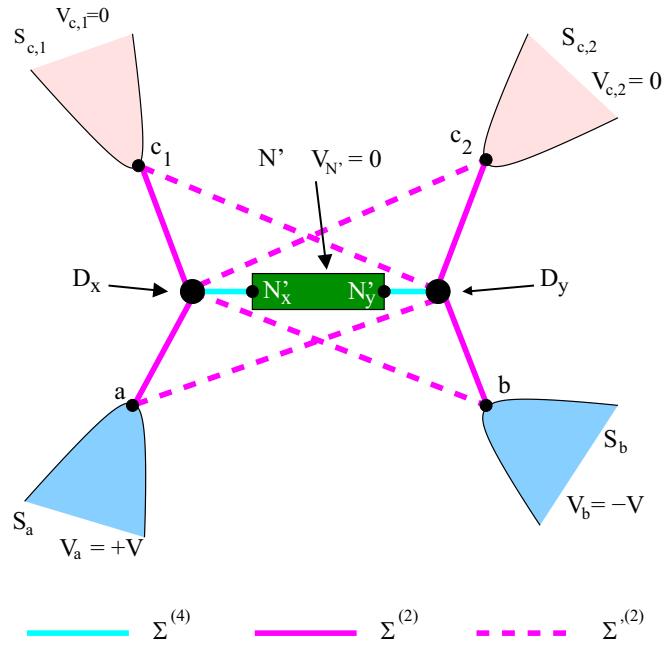

FIG. 4. The four-terminal phenomenological model of superconducting double 0D quantum dot with normal lead in series. The figure shows a double 0D quantum dot connected to the four superconducting leads S_a, S_b, $S_{c,1}$, and $S_{c,2}$ biased at $V_{a,b} = \pm V$ and $V_{c,1} = V_{c,2} = 0$, and to the four grounded normal leads N_1, N_2, N_3, and N_4. The corresponding Hamiltonian is provided in Sec. II B 3. The coupling $\Sigma^{(4)}$ [see Eqs. (34)–(36)] couples the two quantum dots D_x and D_y to the conductor N' that, in the calculations, is characterized by the local and nonlocal Green's functions among the tight-binding sites N_x and N_y. The "direct" coupling $\Sigma^{(2)}$ connects D_x to S_a, D_x to $S_{c,1}$, D_y to S_b, and D_y to $S_{c,2}$ [see Eqs. (21)–(25)]. The "crossed" coupling $\Sigma'^{(2)}$ connects D_x to S_b, D_x to $S_{c,2}$, D_y to S_a, and D_y to $S_{c,1}$ [see Eqs. (26)–(30)]. This model will be used in Secs. III B 1, III B 2, III B 3, III C, and V.

As in the above Sec. II B 2, the quantum dots D_x and D_y have the vanishingly small Hamiltonians of Eqs. (9) and (10), the superconducting leads S_a, S_b, $S_{c,1}$, and $S_{c,2}$ are described by the BCS Hamiltonian given by Eq. (1) and the normal lead is described by Eq. (11). Tunneling between the leads S_a, S_b, $S_{c,1}$, and $S_{c,2}$ and the double quantum dot (D_x, D_y) is described by the same single-channel contacts as in the above Eqs. (21)–(24). In addition, the crossed tunneling amplitudes given by Eqs. (26)–(29) are also included for completeness.

The coupling to the normal lead is phenomenologically accounted for by replacing the tunneling amplitude $\Sigma^{(0)}$ between the quantum dots by propagation through the normal conductor N' connected to the dots D_x and D_y by the single-channel tunneling amplitudes $\Sigma^{(0)}_{D_x,N'_x}$ and $\Sigma^{(0)}_{D_y,N'_y}$, respectively:

$$\mathscr{H}_{T,D_x,N'_x} = -\Sigma^{(4)}_{D_x,N'_x} \sum_{\sigma_z} c^{+}_{N'_x,\sigma_z} c_{D_x,\sigma_z} + \text{H.c.}, \tag{34}$$

$$\mathscr{H}_{T,D_y,N'_y} = -\Sigma^{(4)}_{D_y,N'_y} \sum_{\sigma_z} c^{+}_{N'_y,\sigma_z} c_{D_y,\sigma_z} + \text{H.c.}, \tag{35}$$

where we assume

$$\Sigma^{(4)}_{D_x,N'_x} = \Sigma^{(4)}_{N'_x,D_x} = \Sigma^{(4)}_{D_y,N'_y} = \Sigma^{(4)}_{N'_y,D_y} \equiv \Sigma^{(4)}. \quad (36)$$

The normal conductor N' is characterized by the local Green's functions at N'_x or N'_y, in addition to nonlocal ones from N'_x to N'_y or from N'_y to N'_x across N'. The nonlocal Green's function between N'_x and N'_y generally has to be a complex number.

This model will be used in Secs. III B 1, III B 2, III B 3, III C, and V.

Physical remarks. Within this phenomenological model of double 0D quantum dot with normal lead in series, the quartet critical current at resonance is sensitive to the Green's function connecting the two quantum dots D_x and D_y. This Green's function is itself sensitive to the microscopic details of the model, i.e., on the value of the separation R_0 between the tight-binding sites N'_x and N'_y within the interval $[R'_0 - \lambda_F/2, R'_0 + \lambda_F/2]$, where λ_F is the Fermi wavelength. Thus, this phenomenological model of double 0D quantum dot with normal lead in series produces strong sample-to-sample fluctuations of the quartet current, where different samples correspond to different values of R_0.

Once disconnected from the superconducting or normal leads, this phenomenological model of double 0D quantum dot with normal lead in series also yields the pair of energy levels that is central to the two-Cooper-pair resonance.

In Sec. V, we present numerical results for this model in the regime of strong sample-to-sample fluctuations.

4. Further physical remarks on the choice of a model

Now, we explain why we focus on the double quantum dot Hamiltonians presented in the Secs. II B 2 and II B 3, instead of a single, three, or four quantum dot Hamiltonians.

First, we comparatively examine single and double 0D quantum dots. At equilibrium, the ABS of a single 0D quantum dot have energy scale Γ typically set by $\Gamma = \Sigma^2/W$, where Σ is the tunneling amplitude between the dot and the superconducting leads. It turns out that, at small Γ, the quasiadiabatic regime $V \lesssim V_*$ with $eV_* \sim \Gamma$, does not produce enhanced quartet critical current according to the forthcoming Sec. III C where the two-Cooper-pair resonance is put in correspondence with nonadiabatic effects.

At equilibrium, double 0D quantum dots are characterized by levels at the opposite energies $\pm\Omega$, where Ω is set by the tunneling amplitude $\Sigma^{(0)}$ between the dots [see Eq. (8)]. Then, the voltage energy $eV_* = \Omega$ of the first resonance remains finite in the weak coupling limit, which implies nonadiabatic behavior and enhancement of the quartet critical current at low V if Ω is small compared to the superconducting gap Δ.

Double 0D quantum dots are thus better candidates than single 0D quantum dots to produce large quartet critical current at small-bias voltage because the two-Cooper-pair resonance is also there in the weak coupling regime of small Γ (see also the forthcoming Sec. VI).

The interest of double 0D quantum dots is also related to the observation that the corresponding four energy levels can accommodate the four fermions of a quartet as a "real state." In this sense, the double 0D quantum dots have the "minimal complexity" in comparison with three or four quantum dot devices.

III. MECHANISM FOR THE TWO-COOPER-PAIR RESONANCE

In this section, we present a general mechanism for emergence of the two-Cooper-pair resonance. We start in Sec. III A with introducing the three-terminal N_a-dot-S_c-dot-N_b Cooper pair beam splitters, and the S_a-dot-S_c-dot-S_b three-terminal Josephson junctions. Next, we calculate effective non-Hermitian self-energies and Hamiltonians in Sec. III B. The transport formulas are discussed in Sec. III C in connection with emergence of resonances. Current conservation is discussed in Sec. III D.

A. Three-terminal two-Cooper-pair resonance

In this section, we introduce the two-Cooper-pair resonance in three-terminal Josephson junctions, i.e., in S_a-dot-S_c-dot-S_b devices, starting with nonlocal resonances in the three-terminal N_a-dot-S_c-dot-N_b.

Figures 5(a)–5(c) show the condition for nonlocal resonance of elastic cotunneling (EC) [38–51] in N_a-dot-S_c-dot-N_b Cooper pair beam splitters. EC transfers single-particle states from N_a to N_b across S_c, and contributes to negative nonlocal conductance $\mathscr{G}_{a,b} = \partial I_a/\partial V_b$ on the voltage biasing condition $V_a = -V_b$, where I_a is the current transmitted into the normal lead N_a. EC is resonant if both quantum dots D_x and D_y have levels at the same energy $\varepsilon_x = \varepsilon_y$, where $\omega = \varepsilon_x = \varepsilon_y$ is the energy of the incoming electron in Fig. 5(a).

Figures 5(d)–5(f) show CAR [38–51] in N_a-dot-S_c-dot-N_b Cooper pair beam splitters, which reflects by nonlocal Andreev reflection spin-up electron impinging from N_a as spin-down hole transmitted into N_b, leaving a Cooper pair in the central S_c. CAR contributes for positive value to the nonlocal conductance $\mathscr{G}_{a,b}$ at the bias voltages $V_a = V_b$ and $V_c = 0$. The nonlocal CAR resonance is obtained if the quantum dots D_x and D_y have levels at the opposite energies $\varepsilon_x = -\varepsilon_y \equiv \omega$.

Considering S_a-dot-S_c-dot-S_b three-terminal Josephson junctions, Figs. 5(g)–5(i) feature double elastic cotunneling (dEC) [41,43,46], which transfers Cooper pairs from S_a to S_b across S_c at the bias voltages $V_a = V_b$. This process is resonant if $\omega = E_0$ (for the spin-up electron crossing D_x or D_y) and $-\omega + 2eV = -E_1$ (for the spin-down hole crossing D_x or D_y). Thus, dEC is resonant if $eV = (E_0 - E_1)/2$ and $\omega = E_0$.

Concerning double crossed Andreev reflection (dCAR) in S_a-dot-S_c-dot-S_b three-terminal Josephson junctions in Figs. 5(j)–5(l), two Cooper pairs from S_a and S_b biased at the voltages $\pm V$ cooperatively enter the grounded S_c, producing transient correlations among four fermions, i.e., the so-called quartets. Then,

$$\omega = E_0, \quad (37)$$

$$-\omega + 2eV = -E_1 \quad (38)$$

are obtained at resonance. Conversely, the same Eqs. (37) and (38) are obtained for resonance of the spin-up electron and spin-down holes crossing D_y.

Now, we assume that D_x and D_y are gathered into a single multilevel quantum dot. Assuming the opposite energies $E_0 = -E_1 \equiv \Omega$ implies $\omega = \Omega$ and $-\omega + 2eV = \Omega$, which yields

$$eV = \omega = \Omega \quad (39)$$

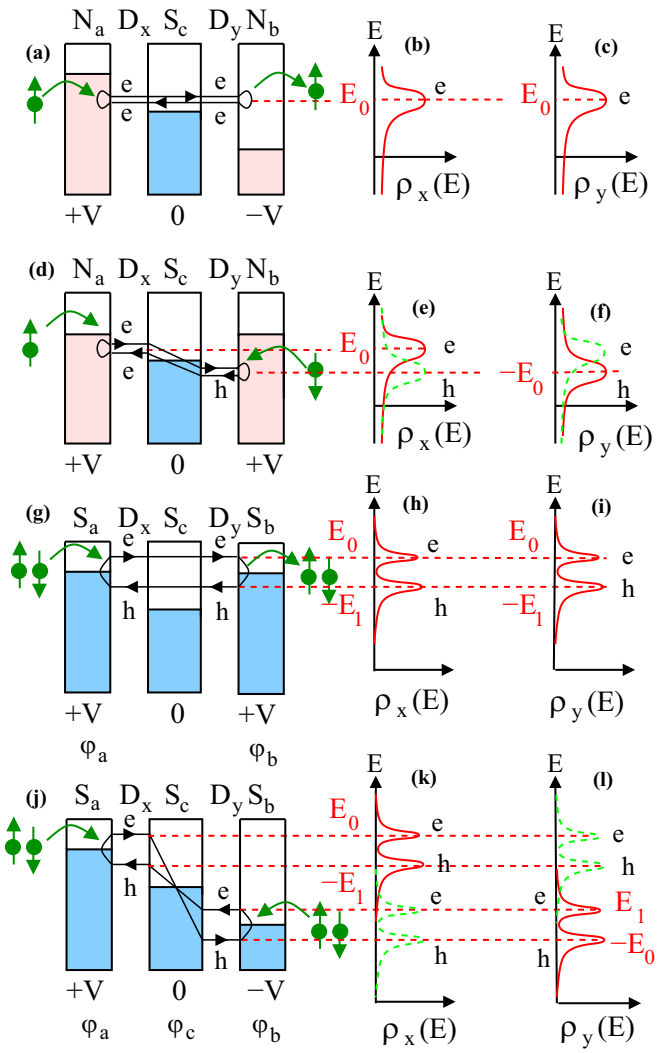

FIG. 5. The nonlocal resonances in three-terminal devices. Panels (a), (d), (g), and (j) show the lowest-order diagrams of elastic cotunneling (EC), crossed Andreev reflection (CAR), double elastic cotunneling (dEC), and double crossed Andreev reflection (dCAR), respectively. Panels (b), (e), (h), and (k) show the energy E dependence of the density of states $\rho_x(E)$ on the quantum dot D_x and (c), (f), (i), and (l) show the corresponding $\rho_y(E)$ on the quantum dot D_y. Panels (e), (f), (k), and (l) also show for completeness by green dashed lines the complementary resonances that do not directly contribute to the corresponding transport processes.

for the nonlocal quartet resonance. Overall, the argument leading to Eq. (39) confirms that nonlocal quartet resonance is produced at voltage energy eV that can be much smaller than the superconducting gap Δ, if the energy scales $\pm\Omega$ are also within $\pm\Delta$ (see also the preceding Sec. II B 4).

B. Effective non-Hermitian self-energy and Hamiltonian

In this section, we present how effective non-Hermitian self-energies or Hamiltonians can be obtained in the infinite-gap limit from the models presented in Sec. II. We start in Sec. III B with the Dyson equations for the three models presented in the Secs. IIB1, II B 2, and II B 3. Emergence of non-Hermitian self-energy in the infinite-gap limit is discussed in Sec. III B 2. Non-Hermitian Hamiltonians are next presented for double quantum dots in the infinite-gap limit (see Sec. III B 3).

1. Closing the Dyson equations

In this section, we provide the starting-point Dyson equations. We adopt a general viewpoint on the three models of Secs. IIB1, II B 2, and II B 3, i.e., multilevel quantum dots, double 0D quantum dots connected in parallel and in series, respectively (see also Figs. 2–4).

The "quantum dot D" is coupled to p_0 superconducting leads labeled by $n_p = 1, \ldots, p_0$ and to q_0 normal leads labeled by $n_q = 1, \ldots, q_0$, where $p_0 = q_0 = 4$ are used in Fig. 2. The Dyson equations take the form

$$\hat{G}_{D,D} = \hat{g}_{D,D} + \sum_{n_q=1}^{q_0}\sum_{n_{q'}=1}^{q_0} \hat{g}_{D,D}\hat{\Sigma}^{(5)}_{D,N_{n_q}}\hat{g}_{N_{n_q},N_{n_{q'}}}\hat{\Sigma}^{(5)}_{N_{n_{q'}},D}\hat{G}_{D,D} + \sum_{n_p=1}^{p_0} \hat{g}_{D,D}\hat{\Sigma}^{(5)}_{D,S_{n_p}}\hat{g}_{S_{n_p},S_{n_p}}\hat{\Sigma}^{(5)}_{S_{n_p},D}\hat{G}_{D,D}. \quad (40)$$

The notation "D" in Eq. (40) refers to the collection of the tight-binding sites in absence of coupling to the superconducting or normal leads, and to the direct coupling between them. For instance, D represents finite-size tight-binding multilevel quantum dot (see Sec. IIB1) or D_x-D_y double quantum dot (see Secs. II B 2 and II B 3). The notation $\Sigma^{(5)}$ denotes generic hopping amplitude, with the normal lead N_{n_q} (corresponding to $\hat{\Sigma}^{(5)}_{D,N_{nq}} = \hat{\Sigma}^{(5)}_{N_{nq},D}$), or with the superconducting lead S_{n_p} (corresponding to $\hat{\Sigma}^{(5)}_{D,S_{n_p}} = \hat{\Sigma}^{(5)}_{S_{n_p},D}$).

The notations $\hat{g}_{N_{n_q},N_{n_{q'}}}$ and $\hat{g}_{S_{n_p},S_{n_p}}$ stand for the bare Green's functions of the normal or superconducting leads N_{n_q}, $N_{n_{q'}}$, or S_{n_p}, respectively, and $\hat{g}_{D,D}$, $\hat{G}_{D,D}$ are the bare and fully dressed quantum dot Green's functions. The bare Green's functions are given by

$$\hat{g}^{A,1,1}_{D,D,\mathbf{x},\mathbf{y}} = \sum_{\psi}\langle\mathbf{x}|\psi\rangle\frac{1}{\omega-\varepsilon_\psi-i\eta}\langle\psi|\mathbf{y}\rangle, \quad (41)$$

$$\hat{g}^{A,2,2}_{D,D,\mathbf{x},\mathbf{y}} = \sum_{\psi}\langle\mathbf{x}|\psi\rangle\frac{1}{\omega+\varepsilon_\psi-i\eta}\langle\psi|\mathbf{y}\rangle, \quad (42)$$

where ω is the real part of the energy and "1,1", "2,2" refer to the electron-electron and hole-hole channels, respectively. In addition, $\hat{g}^{A,1,2}_{D,D,\mathbf{x},\mathbf{y}} = \hat{g}^{A,2,1}_{D,D,\mathbf{x},\mathbf{y}} = 0$ because of the absence of superconducting pairing on the quantum dot. The Dynes parameter η in Eqs. (41) and (42) [32–35] makes the distinction between the advanced and retarded Green's functions, and it can be used to capture relaxation on the quantum dot [83,122]. As in the previous Eq. (11), the notation $|\psi\rangle$ in Eqs. (41) and (42) stands for the single-particle states, and $\langle\mathbf{x}|\psi\rangle$, $\langle\mathbf{y}|\psi\rangle$ are the corresponding wave functions at the tight-binding sites $\mathbf{x}$ and $\mathbf{y}$.

The bare and fully dressed Green's functions $\hat{g}_{D,D}$ and $\hat{G}_{D,D}$ have entries in the Nambu labels, and in the tight-binding sites making the contacts between the dot and the normal or superconducting leads N_{n_q} or S_{n_p}. In addition, those matrices have entries in the set of the harmonics of the Josephson frequency.

2. *Effective non-Hermitian self-energy*

In this section, we explain how effective non-Hermitian self-energy is obtained in the infinite-gap limit. It was already mentioned in the Introduction section that the infinite-gap limit was introduced and considered over the last few years (see, for instance, Refs. [18,36,37] to cite but a few).

Specifically, Eq. (40) is rewritten as

$$\Bigg[\hat{g}^{-1}_{D,D}(\omega) - \sum_{n_q=1}^{q_0}\sum_{n_{q'}=1}^{q_0} \hat{\Sigma}^{(5)}_{D,N_{n_q}} \hat{g}_{N_{n_q},N_{n_{q'}}} \hat{\Sigma}^{(5)}_{N_{n_{q'}},D} - \sum_{n_p=1}^{p_0} \hat{\Sigma}^{(5)}_{D,S_{n_p}} \hat{g}_{S_{n_p},S_{n_p}} \hat{\Sigma}^{(5)}_{S_{n_p},D}\Bigg] \hat{G}_{D,D}(\omega) = \hat{I}. \tag{43}$$

In addition, $\hat{g}_{S,S}$ is independent on ω in the considered infinite-gap limit, and the local Green's function $\hat{g}_{N_{n_q},N_{n_{q'}}}$ in the normal leads is also taken as being independent on energy.

Then, Eq. (43) can be rewritten as

$$[\omega - \hat{\Sigma}_{\text{Non-Her.}}(\omega)]^{-1} \hat{G}_{D,D}(\omega) = \hat{I}, \tag{44}$$

where the self-energy

$$\hat{\Sigma}_{\text{Non-Her.}}(\omega) = \omega - \hat{g}^{-1}_{D,D}(\omega) + \sum_{n_q=1}^{q_0}\sum_{n_{q'}=1}^{q_0} \hat{\Sigma}^{(5)}_{D,N_{n_q}} \hat{g}_{N_{n_q},N_{n_{q'}}} \hat{\Sigma}^{(5)}_{N_{n_{q'}},D} + \sum_{n_p=1}^{p_0} \hat{\Sigma}^{(5)}_{D,S_{n_p}} \hat{g}_{S_{n_p},S_{n_p}} \hat{\Sigma}^{(5)}_{S_{n_p},D} \tag{45}$$

is non-Hermitian, due to $\hat{g}_{N_{n_q},N_{n_{q'}}}$.

3. *Specializing to double quantum dots*

In this section, we discuss emergence of non-Hermitian Hamiltonian for the phenomenological model of double 0D quantum dots. The normal leads in parallel (see Sec. II B 2) are treated in the same framework as normal leads in series (see Sec. II B 3).

The retarded and advanced Green's functions $\sim 1/(\omega - \mathscr{H}^R_{\text{eff}})$ and $\sim 1/(\omega - \mathscr{H}^A_{\text{eff}})$ are obtained from the effective non-Hermitian Hamiltonians $\mathscr{H}^R_{\text{eff}} \equiv \mathscr{H}_{\text{eff}}$ and $\mathscr{H}^A_{\text{eff}} = (\mathscr{H}_{\text{eff}})^+$, respectively. Their complex eigenvalues receive interpretation of the real and imaginary parts of the ABS energies, yielding coherent oscillations and damping in the ABS dynamics, respectively.

We make use of the same compact notations as in the previous Secs. III B 1 and III B 2. Then we show that the effective non-Hermitian self-energy $\hat{\Sigma}_{\text{Non-Her.}}(\omega)$ in Eq. (45) becomes energy independent for those double 0D quantum dots, thus defining the effective non-Hermitian Hamiltonian $\hat{\mathscr{H}}^{(\infty)}_{\text{eff}} \equiv \hat{\Sigma}_{\text{Non-Her.}}$ in the infinite-gap limit.

The matrices in Eq. (43) have entries in the tight-binding sites at the boundary of the quantum dot, where the tunneling self-energy between the dot and the superconducting or normal leads is acting. The boundary is identical to the bulk for the double 0D quantum dots D_x-D_y isolated from the leads. Thus, $g_{D,D}$ takes the value

$$\hat{g}^R_{D,D} = (\omega + i\eta - \hat{\mathscr{H}}_{\text{dot}})^{-1}, \tag{46}$$

where $\hat{\mathscr{H}}_{\text{dot}}$ is the double 0D quantum dot Hamiltonian. The retarded Green's functions of the double 0D quantum dots with normal leads in parallel (see Fig. 3) can then be expressed as

$$\hat{G}^R_{D,D} = \left(\omega + i\eta - \hat{\mathscr{H}}^{(\infty)}_{\text{eff}}\right)^{-1}, \tag{47}$$

where the infinite-gap-limit effective Hamiltonian

$$\hat{\mathscr{H}}^{(\infty)}_{\text{eff}} = \hat{\mathscr{H}}_{\text{dot}} + \sum_{n_q=1}^{q_0}\sum_{n_{q'}=1}^{q_0} \hat{\Sigma}^{(5)}_{D,N_{n_q}} \hat{g}_{N_{n_q},N_{n_{q'}}} \hat{\Sigma}^{(5)}_{N_{n_{q'}},D} + \sum_{n_p=1}^{p_0} \hat{\Sigma}^{(5)}_{D,S_{n_p}} \hat{g}_{S_{n_p},S_{n_p}} \hat{\Sigma}^{(5)}_{D_{n_p},D} \tag{48}$$

is non-Hermitian, due to $\hat{g}_{N_{n_q},N_{n_{q'}}}$.

We note that infinite-gap Hamiltonians can more generally be deduced from the self-energy $\hat{\Sigma}_{\text{Non-Her.}}(\omega)$ in Eq. (45) by extending the domain of definition of the tunneling amplitude to all tight-binding sites of the quantum dots, and associating vanishingly small tunneling amplitudes to those fictitious superconducting leads.

C. Emergence of resonances in the transport formula

In this section, we demonstrate that the current at resonance is inverse proportional to the damping rate. Using the same notations as in the previous Secs. III B 1, III B 2, and III B 3, the current flowing from the multilevel quantum dot into the superconducting lead S_{n_p} is given by the following energy integral [10,11,123,124]:

$$I_{D,S_{n_p}} = \frac{e}{\hbar}\int d\omega \text{Tr}\{\hat{\sigma}^z_N[\hat{\Sigma}^{(5)}_{D,S_{n_p}} \hat{G}^{+,-}_{S_{n_p},D} - \hat{\Sigma}^{(5)}_{S_{n_p},D} \hat{G}^{+,-}_{D,S_{n_p}}]\}, \tag{49}$$

where the Pauli matrix $\hat{\sigma}^z_N$ is defined as $\hat{\sigma}^z_N = \text{diag}(1,-1)$ on the set of the Nambu labels, which is referred to as the subscript "N" for "Nambu." In Eq. (49), $\hat{G}^{+,-}$ is the fully dressed Keldysh Green's function (see Refs. [11,123,124]). The bare superconducting Green's functions $\hat{g}^{+,-}_{S_{n_p},S_{n_p}} = 0$ are vanishingly small if the infinite-gap limit is taken, and $\hat{g}^{+,-}_{N_{n_q},N_{n'_q}} \neq 0$ is nonvanishingly small in the normal leads, due the corresponding finite value of the normal density of states.

The two terms $\hat{\Sigma}^{(5)}_{D,S_{n_p}} \hat{G}^{+,-}_{S_{n_p},D}$ and $\hat{\Sigma}^{(5)}_{S_{n_p},D} \hat{G}^{+,-}_{D,S_{n_p}}$ in Eq. (49) can be expanded as follows:

$$\hat{\Sigma}^{(5)}_{D,S_{n_p}} \hat{G}^{+,-}_{S_{n_p},D} = \sum_{q,q'} \hat{\Sigma}^{(5)}_{D,S_{n_p}} [\hat{I} + \hat{G}^R \hat{\Sigma}^{(5)}]_{S_{n_p},N_q} \hat{g}^{+,-}_{N_q,N_{q'}} [\hat{I} + \hat{\Sigma}^{(5)} \hat{G}^A]_{N_{q'},D}, \tag{50}$$

$$\hat{\Sigma}^{(5)}_{S_{n_p},D} \hat{G}^{+,-}_{D,S_{n_p}} = \sum_{q,q'} \hat{\Sigma}^{(5)}_{S_{n_p},D} [\hat{I} + \hat{G}^R \hat{\Sigma}^{(5)}]_{D,N_q} \hat{g}^{+,-}_{N_q,N_{q'}} [\hat{I} + \hat{\Sigma}^{(5)} \hat{G}^A]_{N_{q'},S_{n_p}}, \tag{51}$$

where N_q and $N_{q'}$ run over the interfaces between the quantum dot and the normal lead.

Then, Eqs. (49)–(51) become

$$I_{D,S_{np}} = \frac{e}{\hbar}\int d\omega \mathrm{Tr}\big\{\hat{\sigma}_N^z\big[\hat{\Sigma}^{(5)}_{D,S_{np}}\hat{g}^R_{S_{np},S_{np}}\hat{\Sigma}^{(5)}_{S_{np},D}\hat{G}^R_{D,D}\hat{\Gamma}^{+,-,N}_{D,D}\hat{G}^A_{D,D} - \hat{\Sigma}^{(5)}_{S_{np},D}\hat{G}^R_{D,D}\hat{\Gamma}^{+,-,N}_{D,D}\hat{G}^A_{D,D}\hat{\Sigma}^{(5)}_{D,S_{np}}\hat{g}^R_{S_{np},S_{np}}\big]\big\}, \tag{52}$$

where

$$\hat{\Gamma}^{+,-,N}_{D,D} = \sum_{n_q=1}^{q_0}\sum_{n_{q'}=1}^{q_0}\hat{\Sigma}^{(5)}_{D,N_{nq}}\hat{g}^{+,-}_{N_{nq},N_{n_{q'}}}\hat{\Sigma}^{(5)}_{N_{n_{q'}},D} \tag{53}$$

is diagonal in Nambu and in Floquet.

The retarded and advanced Green's functions are approximated as [84,116]

$$\hat{G}^R_{D,D} \simeq \sum_{k',l'}\frac{\hat{R}^R_{k',l'}}{\omega - k'eV - E_{l'} + i\delta_{l'}}, \tag{54}$$

$$\hat{G}^A_{D,D} \simeq \sum_{k'',l''}\frac{\hat{R}^A_{k'',l''}}{\omega - k''eV - E_{l''} - i\delta_{l''}}, \tag{55}$$

where k', l', k'', and l'' are four integers, $E_{l'}$, $E_{l''}$ and $\delta_{l'}$, $\delta_{l''}$ are the Floquet energies and linewidth broadening, and $\hat{R}^R_{k',l'}$, $\hat{R}^A_{k'',l''}$ are the matrix residues. Then, inserting Eqs. (54) and (55) into Eq. (52) and integrating over the energy ω yields

$$I_{D,S_{np}} = \frac{\pi e}{2\hbar}\sum_{(k,l)}\frac{1}{\delta_l}\mathrm{Tr}\big\{\hat{\sigma}_N^z\big[\hat{\Sigma}^{(5)}_{D,S_{np}}\hat{g}_{S_{np},S_{np}}\hat{\Sigma}^{(5)}_{S_{np},D}, \hat{R}^R_{k,l}\hat{\Gamma}^{+,-,N}_{D,D}\hat{R}^A_{k,l}\big]_-\big\}, \tag{56}$$

where $[\ldots,\ldots]_-$ is a commutator and $\sum_{(k,l)}$ denotes summation over the pairs of labels k and l such that

$$k'eV + E_{l'} = k''eV + E_{l''} \equiv keV + E_l. \tag{57}$$

Thus, we find that the current is inverse proportional to the damping rate set by the parameter δ_l.

D. Current conservation

Now, we consider that the effective non-Hermitian Hamiltonian with complex eigenvalues originates from the Hermitian Hamiltonians presented in Sec. II (see also Appendix A). It turns out that the total current is conserved once the fraction of the current transmitted into the normal lead has been taken into account. Current conservation can be demonstrated by assuming that the average number of fermions $\langle\hat{N}_{\mathrm{dot}}\rangle$ on the quantum dot is stationary. The Hamiltonian $\mathscr{H}$ can be written as a sum of the Hamiltonians of the quantum dot, of the lead, and tunneling between them. Then, $d\langle\hat{N}_{\mathrm{dot}}\rangle/dt = 0$ is equivalent to current conservation. Thus, non-Hermitian effective Hamiltonian does not contradict current conservation. We note that self-consistent algorithms were used in Ref. [83] to impose current conservation in three-terminal Josephson junctions in the presence of a phenomenological Dynes parameter η.

IV. MECHANISM FOR THE INVERSION

We discussed in the previous Sec. III how sharp resonance peaks can appear in the voltage dependence of the quartet critical current. Now, we provide simple arguments for the magnetic flux-Φ sensitivity of the quartet critical current in the $V = 0^+$ adiabatic limit, focusing on how the quartet critical current $I_{q,c}(\Phi = 0)$ in zero field $\Phi = 0$ compares to $I_{q,c}(\Phi = \pi)$ at half-flux quantum $\Phi = \pi$. Inversion corresponds to larger quartet critical current at $\Phi = \pi$ than at $\Phi = 0$, i.e., $I_{q,c}(\Phi = \pi) > I_{q,c}(\Phi = 0)$. Absence of inversion corresponds to $I_{q,c}(\Phi = \pi) < I_{q,c}(\Phi = 0)$.

Figure 6 shows a sequence of microscopic processes for the quartets in the presence of the two energy levels $E = \pm\Omega$ on the quantum dot. Figure 6(b) shows spin-up electron at energy $E = \Omega$ on the left part of the two-level quantum dot, and how it moves to the right part. Figure 6(c) shows spin-up electron at energy $E = \Omega$ on the right part of the junction, and how it is converted by Andreev reflection into spin-down hole at energy $E = -\Omega$ at the interface with the $S_{c,2}$ superconducting lead. Figure 6(d) shows the resulting spin-down hole at energy $E = -\Omega$, together with a Cooper pair taken from S_b. Figure 6(e) shows the resulting spin-up electron at energy $E = -\Omega$ on the right part of the quantum dot, and how it moves to the left part. Figure 6(f) shows spin-up electron at energy $E = -\Omega$ on the left part of the junction, and how it is converted into spin-down hole at energy $E = \Omega$ by Andreev reflection at the interface with $S_{c,1}$. Figure 6(g) shows the resulting spin-down hole on the left part of the junction at the energy $E = \Omega$, together with absorption of a Cooper pair taken from S_a, thus coming back to the initial state in Fig. 6(b).

Overall, the transition between Figs. 6(b) and 6(c) implies negative sign for the "split quartets" transmitting a Cooper pair into $S_{c,1}$ and another one into $S_{c,2}$, and a positive sign for the "unsplit quartets," corresponding to two Cooper pairs transmitted into $S_{c,1}$ or into $S_{c,2}$. The resulting opposite signs in the "split" and "unsplit" channels imply the inversion (see our previous Paper I [87]). This physical picture for "emergence of inversion in the $V = 0^+$ limit" is confirmed by the calculations presented in Appendix B 2.

Thus, we demonstrated that "inversion between $\Phi = 0$ and $\Phi = \pi$" or "absence of inversion" is linked to the quantum dot single-particle states, i.e., to the number of nodes in their wave-functions.

V. NUMERICAL RESULTS

In this section, we present a selection of the numerical results for the phenomenological model of double 0D quantum dot with normal lead in series (see Fig. 4 and the Hamiltonian in Sec. II B 3). The quantum dots D_x and D_y are coupled to each other by the tunneling amplitude $\Sigma^{(0)}$ defined in Eq. (8). The coupling $\Gamma = (\Sigma^{(2)})^2/W$ is defined for hopping between D_x and S_a, D_x and $S_{c,1}$, D_y and S_b, D_y and $S_{c,2}$ [see $\Sigma^{(2)}$ in Eq. (25)]. We add the coupling $\Gamma' = (\Sigma'^{(2)})^2/W$ between D_x and S_b, D_x and $S_{c,2}$, D_y and S_a, D_y and $S_{c,1}$ [see $\Sigma'^{(2)}$ in Eq. (30)]. The Green's functions of N' are given by

$$\hat{g}^{1,1}_{N'_x,N'_y} = \hat{g}^{1,1}_{N'_y,N'_x} = A_R + iA_I, \tag{58}$$

$$\hat{g}^{2,2}_{N'_x,N'_y} = \hat{g}^{2,2}_{N'_y,N'_x} = -A_R + iA_I, \tag{59}$$

$$\hat{g}^{1,1}_{N'_x,N'_x} = \hat{g}^{1,1}_{N'_y,N'_y} = B_R + iB_I, \tag{60}$$

$$\hat{g}^{2,2}_{N'_x,N'_x} = \hat{g}^{2,2}_{N'_y,N'_y} = -B_R + iB_I, \tag{61}$$

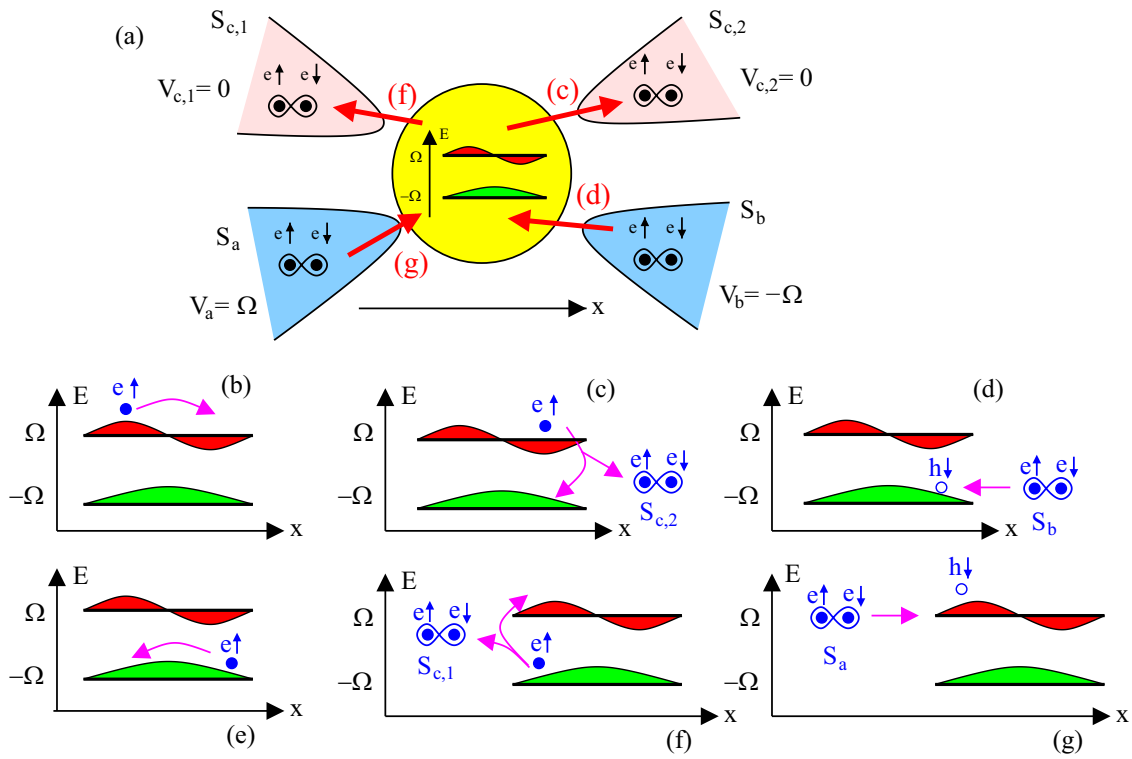

FIG. 6. (a) Schematically shows a quantum dot supporting levels at the opposite energies $E = \pm\Omega$, coupled to the superconducting leads S_a and S_b biased at $eV_{a,b} = \pm\Omega$ and to the grounded $S_{c,1}$ and $S_{c,2}$. (b)–(g) Represent two levels at the opposite energies $\pm\Omega$, together with the corresponding wave functions, with absence of node at $E = -\Omega$, and a node at $E = \Omega$. (b)–(g) Show the time evolution of the quartet process, involving Cooper pair transmitted into $S_{c,2}$ (c), Cooper pair taken from S_b (d), Cooper transmitted into $S_{c,1}$ (f), and Cooper pair taken from S_a (g). Detailed comments about (b)–(g) are given in the text.

where (A_R, A_I) and (B_R, B_I) are four real-valued parameters for the nonlocal and local Green's functions $\hat{g}_{N'_x,N'_y} = \hat{g}_{N'_y,N'_x}$ and $\hat{g}_{N'_x,N'_x}$, $\hat{g}_{N'_y,N'_y}$ respectively, within the assumption $\hat{g}_{N'_x,N'_x} = \hat{g}_{N'_y,N'_y}$. All of the numerical calculations presented below are within the assumption $B_R = B_I = 0$, which is justified as mimicking perfect transmission for highly transparent extended interfaces between the superconductors and the ballistic 2D metal. This assumption yields vanishingly small value for the local Green's function involving "U turn" of the quasiparticle coming back on the interface, a process that is not possible at high transparency in the absence of disorder. In addition to being physically motivated, the condition $B_R = B_I = 0$ allows restricting the parameter space to be explored in the numerical calculations.

The assumption of 0D quantum dots implies that the quartet critical current depends on the value of the Green's function crossing the conductor N' between N'_x and N'_y (see N', N'_x, and N'_y in Fig. 4). The nonlocal Green's function crossing N' oscillates with the combinations $\cos(k_F R_0)$ and $\sin(k_F R_0)$, where R_0 is the separation between N'_x and N'_y, and k_F is the Fermi wave vector. Sharp resonance peaks emerge at fixed $k_F R_0$ in the voltage-V dependence of the quartet current (see the previous Sec. III and the numerical results in the present section. The interplay between those $k_F R_0$ oscillations in space and the sharp Floquet resonances in the voltage dependence of the quartet critical current is expected to produce log-normal distribution of strong sample-to-sample fluctuations, where different samples are characterized by different values of R_0. In this section, we specifically investigate the regime of strong log-normal distribution of sample-to-sample fluctuations and make the physically motivated assumption that fixing A_R, A_I yields quartet critical current-voltage dependence that is qualitatively representative of the signal in this regime of strong sample-to-sample fluctuations.

The codes have been developed over the last few years [82–84,88,91,95,97,116]. They are based on recursive calculations as a function of the harmonics of the Josephson frequency [10,11] (see also the Appendix of Ref. [82]) and on sparse matrix algorithms for matrix products. We specifically adapted the code of our recent Ref. [91] to include the local and nonlocal Green's functions given by Eqs. (58)–(61).

In the forthcoming Figs. 7 and 8, we present numerical results for the voltage dependence of the quartet critical current $I_{q,c}$ defined as

$$\begin{aligned} &I_{q,c}(\Phi = 0, eV/\Delta) \\ &= \max_{\varphi_q}[I_q(\Phi = 0, \varphi_q, eV/\Delta) - I_q(\Phi = 0, -\varphi_q, eV/\Delta)] \\ &- \min_{\varphi_q}[I_q(\Phi = 0, \varphi_q, eV/\Delta) - I_q(\Phi = 0, -\varphi_q, eV/\Delta)], \end{aligned} \tag{62}$$

$$\begin{aligned} &I_{q,c}(\Phi = \pi, eV/\Delta) \\ &= \max_{\varphi_q}[I_q(\Phi = \pi, \varphi_q, eV/\Delta) - I_q(\Phi = \pi, -\varphi_q, eV/\Delta)] \\ &- \min_{\varphi_q}[I_q(\Phi = \pi, \varphi_q, eV/\Delta) - I_q(\Phi = \pi, -\varphi_q, eV/\Delta)]. \end{aligned} \tag{63}$$

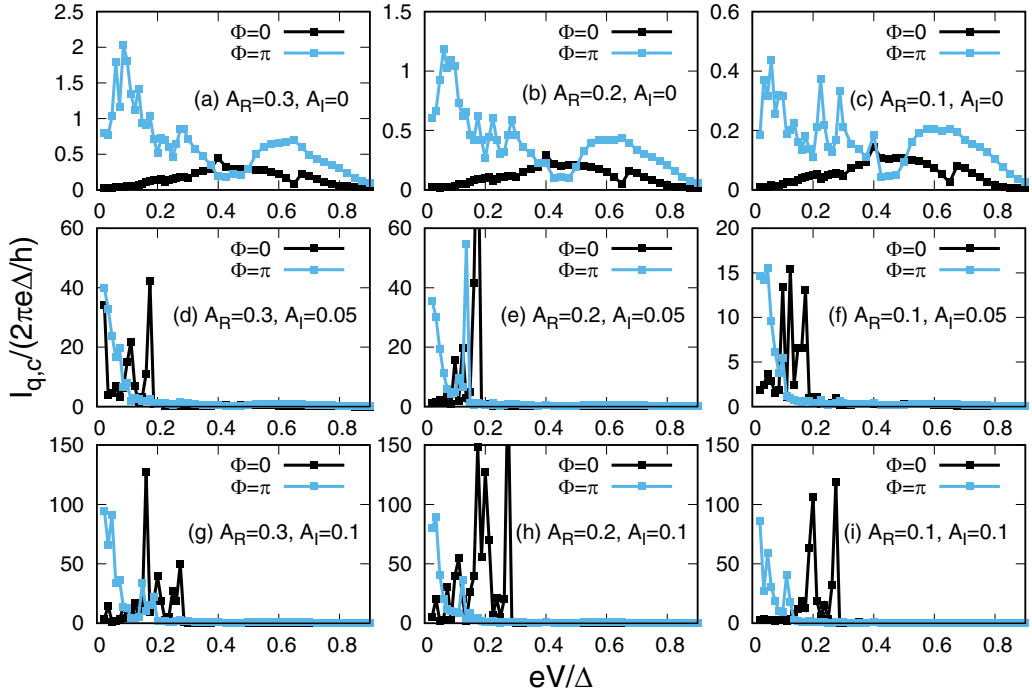

FIG. 7. The eV/Δ dependence of the quartet critical current. Each panel of this figure shows $I_{q,c}(eV/\Delta, \Phi = 0)$ and $I_{q,c}(\Phi = \pi, eV/\Delta)$ as a function of the normalized bias voltage eV/Δ, for $A_I = 0$ and $A_R = 0.3/W$ (a), $A_R = 0.2/W$ (b), and $A_R = 0.1/W$ (c). (d)–(f) Correspond to $A_I = 0.05/W$ and $A_R = 0.3/W$ (d), $A_R = 0.2/W$ (e), and $A_R = 0.1/W$ (f), and (g)–(i) show $I_{q,c}(\Phi = 0, eV/\Delta)$ and $I_{q,c}(\Phi = \pi, eV/\Delta)$ for $A_I = 0.1/W$ and $A_R = 0.3/W$ (g), $A_R = 0.2/W$ (h), and $A_R = 0.1/W$ (i). We use $\Gamma/\Delta = 1$, $\Gamma'/\Delta = 0$, $B_R = B_I = 0$, and $\varepsilon_x = \varepsilon_y = 0$. The notation W is used for the bandwidth.

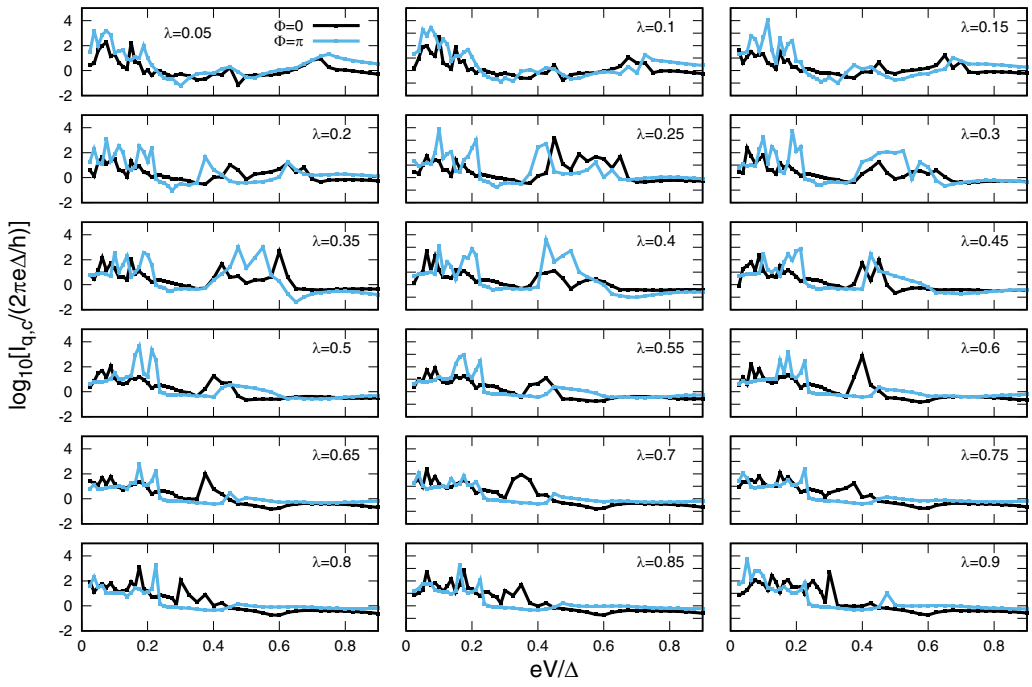

FIG. 8. The eV/Δ dependence of the quartet critical current. The figure shows the reduced voltage-eV/Δ dependence of the logarithm of the quartet critical currents $\log_{10}[I_{q,c}(\Phi = 0, eV/\Delta)]$ and $\log_{10}[I_{q,c}(\Phi = \pi, eV/\Delta)]$ at $\Phi = 0$ and $\Phi = \pi$, respectively. The panels show increasing values of $\lambda = \Gamma'/\Gamma$, where Γ is the "direct" coupling between D_x and S_a, $S_{c,1}$ and between D_y and S_b, $S_{c,2}$. The crossed coupling Γ' is in-between D_x and S_b, $S_{c,2}$ and between D_y and S_a, $S_{c,1}$. We used $\Gamma/\Delta = 1$, $A_R = 0.3/W$, $A_I = 0.05/W$, and $B_R = B_I = 0$, where W is the bandwidth. The onsite energies $\varepsilon_x = \varepsilon_y = 0$ are vanishingly small.

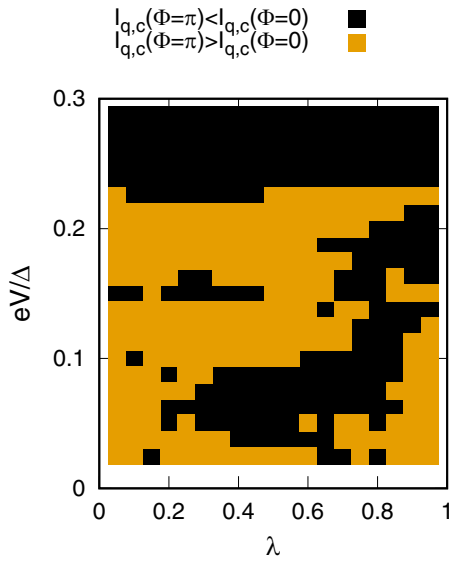

FIG. 9. The sign of the inversion. The figure shows the sign of $I_{q,c}(\lambda, \Phi = \pi, eV/\Delta) - I_{q,c}(\lambda, \Phi = 0, eV/\Delta)$, where $\lambda = \Gamma'/\Gamma$. Inversion corresponds to $I_{q,c}(\lambda, \Phi = \pi, eV/\Delta) - I_{q,c}(\lambda, \Phi = 0, eV/\Delta) > 0$. The parameter Γ is the "direct" coupling between D_x and $(S_a, S_{c,1})$ or between D_y and $(S_b, S_{c,2})$. The parameter Γ' is in-between D_x and $(S_b, S_{c,2})$ or D_y and $(S_a, S_{c,1})$. We used $\Gamma/\Delta = 1$, $A_R = 0.3/W$, $A_I = 0.05/W$, and $B_R = B_I = 0$, where W is the bandwidth. The onsite energies $\varepsilon_x = \varepsilon_y = 0$ are vanishingly small.

In addition, we present color maps for the sign of $I_{q,c}$ as a function of the model parameters (see the forthcoming Figs. 9 and 10).

Figure 7 shows the normalized bias voltage-eV/Δ dependence of the quartet critical currents $I_{q,c}(\Phi = 0, eV/\Delta)$ and $I_{q,c}(\Phi = \pi, eV/\Delta)$ at the flux values $\Phi = 0$ and π. The coupling parameters $\Gamma/\Delta = 1$ and $\Gamma'/\Delta = 0$ are used in Fig. 7.

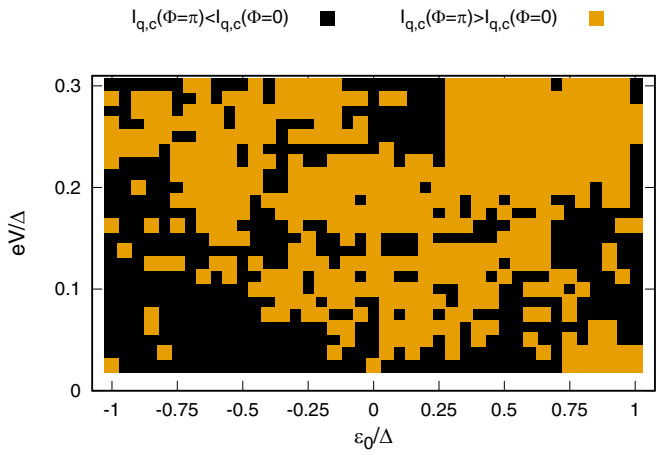

FIG. 10. The sign of the inversion. The figure is similar to the previous Fig. 9, but now the sign of $I_{q,c}(\varepsilon_0/\Delta, \Phi = \pi, eV/\Delta) - I_{q,c}(\varepsilon_0, \Phi = 0, eV/\Delta)$ is shown in the $(\varepsilon_0/\Delta, eV/\Delta)$ plane. We used $\Gamma/\Delta = 1, A_R = 0.3/W, A_I = 0.05/W, B_R = B_I = 0$ (where W is the bandwidth) and $\lambda = \Gamma'/\Gamma = \frac{1}{2}$. The onsite energies are identical for both quantum dots: $\varepsilon_x = \varepsilon_y = \varepsilon_0$.

Figures 7(a)–7(c) correspond to absence of relaxation with $A_I = 0$, producing small quartet critical current. Figures 7(d)–7(i) correspond to the nonvanishingly small relaxation parameters $A_I = 0.05/W$ and $0.1/W$, respectively, producing large quartet critical current at small voltage ratio eV/Δ. In addition, sharp resonances emerge in the variations of the quartet critical current as a function of eV/Δ for $A_I = 0.05/W$ and $A_I = 0.1/W$ in Figs. 7(d)–7(i), respectively. The numerical results in Fig. 7 are in agreement with the general mechanism of Sec. III.

Figure 8 shows the normalized voltage-eV/Δ dependence of the quartet critical current $I_{q,c}$, in semi-logarithmic scale, now with nonvanishingly small $\lambda = \Gamma'/\Gamma$, and with $A_I = 0.05/W$. Those sharp peaks in the quartet critical current are expected to change as the value of the normal metal Green's functions is varied in Eqs. (58)–(61). The quartet critical current plotted as a function of the bias voltage V is normal in log-scale. The corresponding peaks are expected to evolve as $k_F R_0$ is varied and, thus, sample-to-sample fluctuations are expected to have log-normal distribution.

In addition, multiple crossovers are obtained in Fig. 8 between $I_{q,c}(\Phi = \pi, eV/\Delta) - I_{q,c}(\Phi = 0, eV/\Delta) > 0$ (i.e., inversion) and $I_{q,c}(\Phi = \pi, eV/\Delta) - I_{q,c}(\Phi = 0, eV/\Delta) < 0$ (i.e., noninverted behavior) in a low-voltage window.

Figure 9 shows the sign of $I_{q,c}(\lambda, \Phi = \pi, eV/\Delta) - I_{q,c}(\lambda, \Phi = 0, eV/\Delta)$ as a function of the parameters $\lambda = \Gamma'/\Gamma$ (on the x axis) and eV/Δ (on the y axis). Inversion $I_{q,c}(\lambda, \Phi = \pi, eV/\Delta) - I_{q,c}(\lambda, \Phi = 0, eV/\Delta) > 0$ is obtained at low eV/Δ for $\lambda = 0$ (see the previous Sec. IV and Appendix B for a discussion of the inversion in the $eV/\Delta = 0^+$ limit). In Fig. 9, increasing the coupling Γ' between D_x and $(S_b, S_{c,2})$ or between D_y and $(S_a, S_{c,1})$ [in addition to Γ between D_x and $(S_a, S_{c,1})$ or between D_y and $(S_b, S_{c,2})$] makes the double 0D quantum dot behave closer to a pair of single quantum dots. This favors the "noninverted behavior" typical of single quantum dots, as opposed to the "inverted behavior" appearing at $\lambda = \Gamma'/\Gamma = 0$ in a double 0D quantum dot (see Appendix B).

The values $\lambda = \Gamma'/\Gamma$ such that $0.2 \lesssim \lambda \lesssim 0.6$ in Fig. 9 generically yield "inversion" at low-bias voltage V, followed by "absence of inversion" at higher V values. Now, we show that "absence of inversion" can appear at low-bias voltage V if the onsite energies $\varepsilon_x = \varepsilon_y \equiv \varepsilon_0$ in the double quantum dot Hamiltonian given by Eqs. (6) and (7) produce detuning from perfectly opposite levels. Namely, the parameter $\lambda = \Gamma'/\Gamma$ is set to $\lambda = \frac{1}{2}$ in Fig. 10. Moving away from $\varepsilon_0/\Delta = 0$ in Fig. 10 produces typical voltage dependence of $I_{q,c}(\lambda, \Phi = \pi, eV/\Delta) - I_{q,c}(\lambda, \Phi = 0, eV/\Delta)$ with "noninverted behavior" at low $V < V_*$ and "inversion" at higher $V > V_*$ (see, for instance, the moderately small values $-0.5 \lesssim \varepsilon_0/\Delta \lesssim 0.5$ in Fig. 10). With the considered parameters, the ratio eV_*/Δ is in the range $eV_*/\Delta \approx 0.1$. Thus, our model is compatible with the experimental data [97] shown in Fig. 1(b).

VI. LOW-VOLTAGE LIMIT

In this section, we focus on the low-voltage limit and insert in Eq. (52) the equilibrium fully dressed advanced and retarded Green's functions. We present an explanation for why the numerical calculations of the preceding Sec. V suggest

that the linewidth broadening δ_l in Eq. (56) appears to be much smaller than $\sim A_I$ in Eqs. (58)–(61).

As in the previous numerical calculations presented in Sec. V, we consider normal leads in series (see Fig. 4 and the Hamiltonian in Sec. II B 3). The Dyson equations (40) take the form

$$\Big((\omega - i\eta) - \hat{\Gamma}^{(a,a)}_{x,x} - \hat{\Gamma}^{(c_1,c_1)}_{x,x} - \hat{\Gamma}^{(N'_x,N'_x)}_{x,x}\Big)\hat{G}_{x,x} - \hat{\Gamma}^{(N'_x,N'_y)}_{x,y}\hat{G}_{y,x} = \hat{g}_{x,x}, \tag{64}$$

$$\Big((\omega - i\eta) - \hat{\Gamma}^{(b,b)}_{y,y} - \hat{\Gamma}^{(c_1,c_1)}_{y,y} - \hat{\Gamma}^{(N'_y,N'_y)}_{y,y}\Big)\hat{G}_{y,x} - \hat{\Gamma}^{(N'_y,N'_x)}_{y,x}\hat{G}_{x,x} = 0, \tag{65}$$

with

$$\hat{\Gamma}^{(a,a)}_{x,x} = -\Gamma_a\begin{pmatrix} 0 & \exp(i\varphi_a) \\ \exp(-i\varphi_a) & 0 \end{pmatrix}, \tag{66}$$

$$\hat{\Gamma}^{(c_1,c_1)}_{x,x} = -\Gamma_{c_1}\begin{pmatrix} 0 & \exp(i\varphi_{c,1}) \\ \exp(-i\varphi_{c,1}) & 0 \end{pmatrix}, \tag{67}$$

$$\hat{\Gamma}^{(b,b)}_{y,y} = -\Gamma_b\begin{pmatrix} 0 & \exp(i\varphi_b) \\ \exp(-i\varphi_b) & 0 \end{pmatrix}, \tag{68}$$

$$\hat{\Gamma}^{(c_2,c_2)}_{y,y} = -\Gamma_{c_2}\begin{pmatrix} 0 & \exp(i\varphi_{c,2}) \\ \exp(-i\varphi_{c,2}) & 0 \end{pmatrix}, \tag{69}$$

where the couplings Γ_a, Γ_b, $\Gamma_{c,1}$, and $\Gamma_{c,2}$ are between the double quantum dot and the superconducting leads S_a, S_b, $S_{c,1}$, and $S_{c,2}$ [see Fig. 4 and the analogous Eqs. (16)–(19)]. In addition, $\hat{\Gamma}^{(N'_x,N'_x)}_{x,x}$, $\hat{\Gamma}^{(N'_x,N'_y)}_{x,y}$, $\hat{\Gamma}^{(N'_y,N'_y)}_{y,y}$, and $\hat{\Gamma}^{(N'_y,N'_x)}_{y,x}$ are given by

$$\hat{\Gamma}^{(N'_x,N'_x)}_{x,x} = \Gamma_{N'_x,N'_x}\begin{pmatrix} W g^{1,1}_{N'_x,N'_x} & 0 \\ 0 & W g^{2,2}_{N'_x,N'_x} \end{pmatrix}, \tag{70}$$

$$\hat{\Gamma}^{(N'_x,N'_y)}_{x,y} = \Gamma_{N'_x,N'_y}\begin{pmatrix} W g^{1,1}_{N'_x,N'_y} & 0 \\ 0 & W g^{2,2}_{N'_x,N'_y} \end{pmatrix}, \tag{71}$$

$$\hat{\Gamma}^{(N'_y,N'_y)}_{y,y} = \Gamma_{N'_y,N'_y}\begin{pmatrix} W g^{1,1}_{N'_y,N'_y} & 0 \\ 0 & W g^{2,2}_{N'_y,N'_y} \end{pmatrix}, \tag{72}$$

$$\hat{\Gamma}^{(N'_y,N'_x)}_{y,x} = \Gamma_{N'_y,N'_x}\begin{pmatrix} W g^{1,1}_{N'_y,N'_x} & 0 \\ 0 & W g^{2,2}_{N'_y,N'_x} \end{pmatrix}, \tag{73}$$

with $\Gamma_{N'_x,N'_x} = (\Sigma_{x,N'_x})^2/W$, $\Gamma_{N'_x,N'_y} = \Sigma_{x,N'_x}\Sigma_{y,N'_y}/W$, $\Gamma_{N'_y,N'_x} = \Sigma_{x,N'_y}\Sigma_{x,N'_x}/W$, $\Gamma_{N'_y,N'_y} = (\Sigma_{x,N'_y})^2/W$, where N'_x and N'_y are the normal-metal tight-binding sites making the contacts with the 0D quantum dots D_x and D_y, respectively.

The Dyson equations (64) and (65) define the infinite-gap Hamiltonian

$$\mathscr{H}^{(\infty)} = \begin{pmatrix} \hat{\Gamma}^{(a,a)}_{x,x} + \hat{\Gamma}^{(c_1,c_1)}_{x,x} + \hat{\Gamma}^{(N'_x,N'_x)}_{x,x} & \hat{\Gamma}^{(N'_x,N'_y)}_{x,y} \\ \hat{\Gamma}^{(N'_y,N'_x)}_{y,x} & \hat{\Gamma}^{(b,b)}_{y,y} + \hat{\Gamma}^{(c_2,c_2)}_{y,y} + \hat{\Gamma}^{(N'_y,N'_y)}_{y,y} \end{pmatrix}, \tag{74}$$

which is now considered in absence of the local couplings $\hat{\Gamma}^{(N'_x,N'_x)}_{x,x} = \hat{\Gamma}^{(N'_y,N'_y)}_{y,y} \equiv 0$, corresponding to the use of $B_R = B_I = 0$ in the above numerical calculations [see the discussion following Eqs. (58)–(61) in Sec. V]. Then, the square of the 4×4 infinite-gap Hamiltonian decouples into a pair of 2×2 blocks (see also Appendix B):

$$\big(\mathscr{H}^{(\infty)}\big)^2 = \begin{pmatrix} \varepsilon^{1,1}_{a,c_1} & 0 & 0 & \kappa_{1,2} \\ 0 & \varepsilon^{2,2}_{a,c_1} & \kappa_{2,1} & 0 \\ 0 & \kappa'_{1,2} & \varepsilon^{1,1}_{b,c_2} & 0 \\ \kappa'_{2,1} & 0 & 0 & \varepsilon^{2,2}_{b,c_2} \end{pmatrix}, \tag{75}$$

with

$$\varepsilon^{1,1}_{a,c_1} = \big|\gamma_{D_x,D_x}\big|^2 + \big(\Gamma_{N'_x,N'_y}\big)^2 W^2 g^{1,1}_{N'_x,N'_y} g^{1,1}_{N'_y,N'_x}, \tag{76}$$

$$\varepsilon^{2,2}_{a,c_1} = \big|\gamma_{D_x,D_x}\big|^2 + \big(\Gamma_{N'_x,N'_y}\big)^2 W^2 g^{2,2}_{N'_x,N'_y} g^{2,2}_{N'_y,N'_x}, \tag{77}$$

$$\varepsilon^{1,1}_{b,c_2} = \big|\gamma_{D_y,D_y}\big|^2 + \big(\Gamma_{N'_x,N'_y}\big)^2 W^2 g^{1,1}_{N'_x,N'_y} g^{1,1}_{N'_y,N'_x}, \tag{78}$$

$$\varepsilon^{2,2}_{b,c_2} = \big|\gamma_{D_y,D_y}\big|^2 + \big(\Gamma_{N'_x,N'_y}\big)^2 W^2 g^{2,2}_{N'_x,N'_y} g^{2,2}_{N'_y,N'_x}, \tag{79}$$

$$\kappa_{1,2} = \Gamma_{N'_x,N'_y} W\Big(g^{2,2}_{N'_x,N'_y}\gamma_{D_x,D_x} + g^{1,1}_{N'_x,N'_y}\gamma_{D_y,D_y}\Big), \tag{80}$$

$$\kappa_{2,1} = \Gamma_{N'_x,N'_y} W\Big(g^{1,1}_{N'_x,N'_y}\overline{\gamma_{D_x,D_x}} + g^{2,2}_{N'_x,N'_y}\overline{\gamma_{D_y,D_y}}\Big), \tag{81}$$

$$\kappa'_{1,2} = \Gamma_{N'_x,N'_y} W\Big(g^{1,1}_{N'_y,N'_x}\gamma_{D_x,D_x} + g^{2,2}_{N'_y,N'_x}\gamma_{D_y,D_y}\Big), \tag{82}$$

$$\kappa'_{2,1} = \Gamma_{N'_x,N'_y} W\Big(g^{2,2}_{N'_y,N'_x}\overline{\gamma_{D_x,D_x}} + g^{1,1}_{N'_y,N'_x}\overline{\gamma_{D_y,D_y}}\Big), \tag{83}$$

where

$$\gamma_{D_x,D_x} = \Gamma_a \exp(i\varphi_a) + \Gamma_{c_1}\exp(i\varphi_{c,1}), \tag{84}$$

$$\gamma_{D_y,D_y} = \Gamma_b \exp(i\varphi_b) + \Gamma_{c_2}\exp(i\varphi_{c,2}). \tag{85}$$

Within each 2×2 block, the eigenvalues take the form

$$\lambda_\pm = \frac{1}{2}\left[\varepsilon^{1,1}_{a,c_1} + \varepsilon^{2,2}_{b,c_2} \pm \sqrt{\big(\varepsilon^{1,1}_{a,c_1} - \varepsilon^{2,2}_{b,c_2}\big)^2 + 4\kappa_{1,2}\kappa'_{2,1}}\right], \tag{86}$$

where the following quantities

$$\varepsilon^{1,1}_{a,c_1} + \varepsilon^{2,2}_{b,c_2} = \big|\gamma_{D_x,D_x}\big|^2 + \big|\gamma_{D_y,D_y}\big|^2 + 2\big(\Gamma_{N'_x,N'_y}\big)^2 W^2\big(A_R^2 - A_I^2\big), \tag{87}$$

$$\begin{aligned}\big(\varepsilon^{1,1}_{a,c_1} - \varepsilon^{2,2}_{b,c_2}\big)^2 + 4\kappa_{1,2}\kappa'_{2,1} &= \Big(\big|\gamma_{D_x,D_x}\big|^2 - \big|\gamma_{D_y,D_y}\big|^2\Big)^2 - 16\big(\Gamma_{N'_x,N'_y}\big)^2 W^2 A_R^2 A_I^2 \\ &\quad + 4\big(\Gamma_{N'_x,N'_y}\big)^2 W^2 A_R^2\big|\gamma_{D_x,D_x} - \gamma_{D_y,D_y}\big|^2 \\ &\quad - 4\big(\Gamma_{N'_x,N'_y}\big)^2 W^2 A_I^2\big|\gamma_{D_x,D_x} + \gamma_{D_y,D_y}\big|^2\end{aligned} \tag{88}$$

are both real valued.

It can also be shown that $\lambda_\pm$ is real valued and positive at small A_I because

$$\big|\gamma_{D_x,D_x}\overline{\gamma_{D_y,D_y}} - \big(\Gamma_{N'_x,N'_y}\big)^2 W^2 g^{1,1}_{N'_x,N'_y} g^{2,2}_{N'_y,N'_x}\big|^2 \tag{89}$$

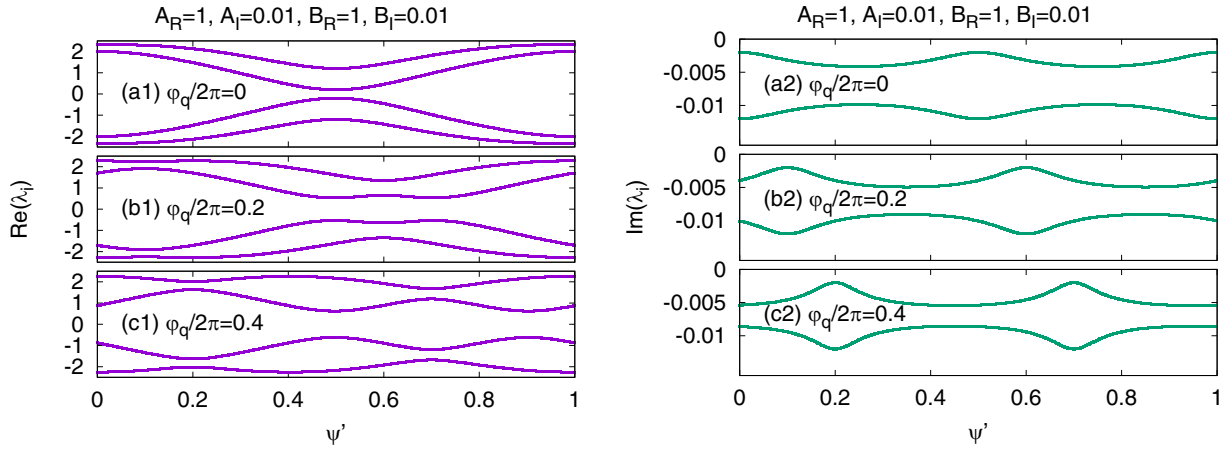

FIG. 11. The real and imaginary parts of the ABS energies in the infinite-gap limit. Panels (a1)–(c1) and (a2)–(c2) show the real and imaginary parts of the ABS energies, respectively, for the 4×4 Hamiltonian given by Eqs. (66)–(74), plotted as a function of the variable ψ' defined as $\varphi_a = \varphi_a^{(0)} + \psi'$, $\varphi_b = \varphi_b^{(0)} - \psi' \varphi_{c,1} = \varphi_c^{(0)}$, and $\varphi_{c,2} = \varphi_c^{(0)}$, with $\varphi_q = \varphi_a^{(0)} + \varphi_b^{(0)} - 2\varphi_c^{(0)}$. The parameters take the general values indicated on the figure, with in addition $\Gamma_a = \Gamma_b = \Gamma_{c,1} = \Gamma_{c,2} = 1$ taken as the unit of energy for the coupling to the superconducting leads, and $\Gamma_{\rm loc} = 0.7$, $\Gamma_{\rm nonloc} = 0.5$ for the "local" and "nonlocal" electron-electron channels [see Eqs. (70)–(73)]. Panels (a2), (b2), and (c2) reveal that $|{\rm Im}(\lambda_i)|$ can be small compared to A_I or B_I (but not orders of magnitude smaller), which implies small δ_l in Eq. (56), and compatibility with the large quartet current reported in the numerical results presented in Sec. V.

is positive, which implies

$$\begin{aligned}
&\left|\gamma_{D_x,D_x}\right|^2\left|\gamma_{D_y,D_y}\right|^2 + \left(\Gamma_{N_x',N_y'}\right)^4 W^4 g^{1,1}_{N_x',N_y'} g^{1,1}_{N_y',N_x'} g^{2,2}_{N_x',N_y'} g^{2,2}_{N_y',N_x'} \\
&> \left(\Gamma_{N_x',N_y'}\right)^2 W^2 g^{1,1}_{N_x',N_y'} g^{2,2}_{N_y',N_x'} \gamma_{D_y,D_y} \overline{\gamma_{D_x,D_x}} \\
&\quad + \left(\Gamma_{N_x',N_y'}\right)^2 W^2 g^{2,2}_{N_x',N_y'} g^{1,1}_{N_y',N_x'} \gamma_{D_x,D_x} \overline{\gamma_{D_y,D_y}}, \qquad (90)
\end{aligned}$$

where we used the approximation $\overline{g^{1,1}_{N_x',N_y'}} \simeq g^{1,1}_{N_x',N_y'}$ and $\overline{g^{2,2}_{N_x',N_y'}} \simeq g^{2,2}_{N_x',N_y'}$ at small A_I. Thus, we obtain

$$\begin{aligned}
&\left(\left|\gamma_{D_x,D_x}\right|^2 + \left(\Gamma_{N_x',N_y'}\right)^2 W^2 g^{1,1}_{N_x',N_y'} g^{1,1}_{N_y',N_x'}\right) \\
&\quad \times \left(\left|\gamma_{D_y,D_y}\right|^2 + \left(\Gamma_{N_x',N_y'}\right)^2 W^2 g^{2,2}_{N_x',N_y'} g^{2,2}_{N_y',N_x'}\right) \\
&> \left(\Gamma_{N_x',N_y'}\right)^2 W^2 \left(g^{2,2}_{N_x',N_y'} \gamma_{D_x,D_x} + g^{1,1}_{N_x',N_y'} \gamma_{D_y,D_y}\right) \\
&\quad \times \left(g^{2,2}_{N_y',N_x'} \overline{\gamma_{D_x,D_x}} + g^{1,1}_{N_y',N_x'} \overline{\gamma_{D_y,D_y}}\right), \qquad (91)
\end{aligned}$$

from what we deduce

$$\left(\varepsilon^{1,1}_{a,c_1} + \varepsilon^{2,2}_{b,c_2}\right)^2 > \left(\varepsilon^{1,1}_{a,c_1} - \varepsilon^{2,2}_{b,c_2}\right)^2 + 4\kappa_{1,2}\kappa'_{2,1} \qquad (92)$$

at small A_I. Then, the eigenvalues $\lambda_\pm$ of the squared infinite-gap Hamiltonian are both real valued at arbitrary A_I [see Eqs. (87) and (88)] and positive at small A_I [see Eq. (92)].

In addition, we carried out complementary numerical calculation for the eigenvalues of the equilibrium 4×4 infinite-gap Hamiltonian defined by Eqs. (66)–(74) (see Fig. 11). We find the possibility of imaginary part of the ABS energies smaller (but not orders of magnitude smaller) than A_I and B_I with general values of the parameters, i.e., not within the above considered $B_R = B_I = 0$ and small A_I. Thus, small δ_l has to be used in Eq. (56) at low-bias voltage, which is compatible with the large quartet current in Fig. 8, similarly to the thermal noise of a superconducting weak link [123].

VII. CONCLUSIONS

Now, we provide final remarks. The paper is summarized in Sec. VII A, and perspectives are presented in Sec. VII B.

A. Summary of the paper

We proposed models of ballistic multiterminal Josephson junctions made with superconducting leads evaporated on a 2D metal. The models consist of multilevel quantum dots connected to superconducting and normal leads. We argued that the qualitative physics of the two-Cooper-pair resonance can be captured with phenomenological double quantum dots connected to superconducting and normal leads. The coupling to the nonproximitized regions of the ballistic conductor produces relaxation, and a fraction of the quartet-phase-sensitive current is transmitted into the normal parts of the circuit.

We found resonances in calculations that account for both the time-periodic dynamics and small relaxation, if the multilevel or double quantum dot support levels at opposite energies. A related effect was previously found in the thermal noise of a superconducting weak link [123]. In addition, we addressed detuning from perfectly opposite energy levels.

Noninverted-to-inverted crossover numerically emerges as the bias voltage increases, where "inversion" means "larger quartet critical current at half flux-quantum $\Phi = \pi$ than in zero field at $\Phi = 0$." The corresponding crossover voltage V_* is small compared to the superconducting gap, typically $eV_* \approx \Delta/10$ with the parameters of our calculations, which is compatible with the recent Harvard group experiment [97].

B. Perspectives

A challenge for the theory is to model devices that are quite complex, with, e.g., extended interfaces, four or more superconducting leads, nonequilibrium voltage-biasing con-

ditions, loops connecting superconducting terminals, possibly with radio-frequency radiation. Direct diagonalizations of the Bogoliubov–de Gennes Hamiltonian would apparently lead to prohibitive computational expenses. In the field of mesoscopic superconductivity, Nazarov and co-workers (see Ref. [125] and references therein) proposed and developed finite element theory for the superconducting–normal-metal circuits that describe the proximity effect, i.e., the interplay between Andreev reflection and multiple scattering on disorder. This dirty-limit circuit theory was proposed for multiterminal Josephson junctions [106,126]. The dirty limit implies short elastic mean-free path, a condition that is not directly met in the ballistic metals that are currently used in some experiments on superconducting hybrid structures, such as carbon nanotubes [127], semiconducting nanowires [102], or graphene [121,128]. Specifically, tunneling spectroscopy of carbon nanotube Josephson junctions [127] revealed discrete ABS. Andreev molecules were realized with semiconducting nanowires [102]. Evidence for superconducting phase-difference-sensitive continuum of ABS was obtained in superconductor-graphene-superconductor Josephson junctions [14,15]. As it is mentioned above, microwave experiments on short superconductor-graphene-superconductor Josephson junctions were recently carried out, and modeled with single-level quantum dots [121].

Several issues related to averaging could be investigated in the future: First, it would be interesting to numerically average over a distribution of the nonlocal Green's function for double 0D quantum dots. A related issue is to implement quantum dots having dimension that is large compared to the Fermi wavelength λ_F instead of the 0D quantum dots of this paper. On the other hand, the "metallic" regime of weak sample-to-sample fluctuations of the quartet critical current can be addressed with quasiclassics. For instance, discretized Usadel equations were used to evaluate multiple Andreev reflections in two-terminal devices in the dirty limit [129] and three-terminal devices were addressed within assumptions about the interface transparencies, also with Usadel equations [78]. Second, the use of Nazarov's circuit theory implies that the Green's function is uniform within a node, which is also satisfied by ballistic chaotic cavities [130]. Thus, Nazarov's circuit theory is also appropriate to describe a ballistic device if the coupling to the terminals is made through interfaces with small cross sections, to ensure that the metal behaves like a chaotic cavity. Third, an interesting perspective is to solve Eilenberger equations for the four-terminal device shown in Fig. 1. Fourth, it would also be interesting to average over voltage fluctuations, the strength of which being controlled by the electromagnetic environment.

To summarize this discussion, perspectives are about the interplay between (i) the "Floquet effects" that produce "non-self-averaging-like" sharp resonance peaks in the voltage dependence of the quartet signal for single-channel contacts, and (ii) the effect of averaging in space over extended contacts or in energy over the voltage fluctuations induced by the electromagnetic environment.

Finally, probability current is conserved in the one-dimensional normal-metal–superconductor junction treated by Blonder, Tinkham, and Klapwijk [131] [see Eqs. (A7) and (A8) in this paper]. We leave as open the question of rigorously discussing probability conservation in the considered four-terminal device connected to normal leads, in connection with introducing the phenomenological Dynes parameter $\eta \neq 0$ and vanishingly small imaginary part of the local Green's function $B_I = 0$ (as it was done here), or with $\eta = 0$ and $B_I \neq 0$ (as it could be done in the future).

To conclude, this paper suggests interest of "quantum bath engineering" multiterminal Josephson junctions in the circuits of cavity-quantum electrodynamics.

ACKNOWLEDGMENTS

The author wishes to thank K. Huang, Y. Ronen, and P. Kim for stimulating discussions about their experiment. The author wishes to thank R. Danneau for useful discussions and comments on the manuscript, and F. Levy-Bertrand and her colleagues H. Cercellier, K. Hasselbach, and M. A. Measson for useful remarks during an informal seminar on this topic. The author thanks the Infrastructure de Calcul Intensif et de Données (GRICAD) for use of the resources of the Mésocentre de Calcul Intensif de l'Université Grenoble-Alpes (CIMENT). The author acknowledges support from the French National Research Agency (ANR) in the framework of the Graphmon project (Grant No. ANR-19-CE47-0007).

APPENDIX A: SPECTRUM IN ABSENCE OF COUPLING TO THE SUPERCONDUCTORS

In this Appendix, we consider the "phenomenological model of double 0D quantum dots with normal lead in series" (see Sec. II B 3) and show that pairs of opposite energies emerge in the spectrum.

We start with the simple limit where the four superconducting leads are disconnected, i.e., $\Gamma = \Gamma' = 0$, and consider that the two quantum dots D_x and D_y are connected to the tight-binding sites N'_x and N'_y by the tunneling amplitudes $\Sigma^{(4)}_{N'_x,D_x} = \Sigma^{(4)}_{D_x,N'_x}$ and $\Sigma^{(4)}_{N'_y,D_y} = \Sigma^{(4)}_{D_y,N'_y}$. The tight-binding sites are self-connected by the Green's functions $g_{N'_x,N'_x}$ and $g_{N'_y,N'_y}$, and connected to each other by the nonlocal Green's functions $g_{N'_x,N'_y} = g_{N'_y,N'_x}$. We denote by $g^A_{D_x,D_x} = g^A_{D_y,D_y} = 1/(\omega - i\eta)$ the Green's functions of the "isolated" quantum dots D_x and D_y [see Eqs. (9) and (10) where $\varepsilon_x = \varepsilon_y = 0$ in Eqs. (6) and (7)]. In addition, $\tilde{g}_{D_x,D_x}$, $\tilde{g}_{D_y,D_y}$ are their counterparts for the connected double 0D quantum dot, and by $\tilde{g}_{D_x,D_y}$ and $\tilde{g}_{D_y,D_x}$ are the corresponding nonlocal Green's functions. The Dyson equations relate the g's to the $\tilde{g}$'s according to

$$\tilde{g}_{D_x,D_x} = g_{D_x,D_x} + g_{D_x,D_x}\Sigma^{(4)}_{D_x,N'_x} g_{N'_x,N'_x}\Sigma^{(4)}_{N'_x,D_x}\tilde{g}_{D_x,D_x} + g_{D_x,D_x}\Sigma^{(4)}_{D_x,N'_x} g_{N'_x,N'_y}\Sigma^{(4)}_{N'_y,D_y}\tilde{g}_{D_y,D_x}, \tag{A1}$$

$$\tilde{g}_{D_y,D_x} = g_{D_y,D_y}\Sigma^{(4)}_{D_y,N'_y} g_{N'_y,N'_x}\Sigma^{(4)}_{N'_x,D_x}\tilde{g}_{D_x,D_x} + g_{D_y,D_y}\Sigma^{(4)}_{D_y,N'_y} g_{N'_y,N'_y}\Sigma^{(4)}_{N'_y,D_y}\tilde{g}_{D_y,D_x}, \tag{A2}$$

which leads to the secular equation

$$\begin{vmatrix} \omega - \Gamma_{D_x,N'_x,N'_x,D_x} & -\Gamma_{D_x,N'_x,N'_y,D_y} \\ -\Gamma_{D_y,N'_y,N'_x,D_x} & \omega - \Gamma_{D_y,N'_y,N'_y,D_y} \end{vmatrix} = 0, \tag{A3}$$

where $\Gamma_{D_x,N'_x,N'_x,D_x} = \Sigma^{(4)}_{D_x,N'_x} g_{N'_x,N'_x} \Sigma^{(4)}_{N'_x,D_x}$, $\Gamma_{D_y,N'_y,N'_y,D_y} = \Sigma^{(4)}_{D_y,N'_y} g_{N'_y,N'_y} \Sigma^{(4)}_{N'_y,D_y}$, $\Gamma_{D_x,N'_x,N'_y,D_y} = \Sigma^{(4)}_{D_x,N'_x} g_{N'_x,N'_y} \Sigma^{(4)}_{N'_y,D_y}$, $\Gamma_{D_y,N'_y,N'_x,D_x} = \Sigma^{(4)}_{D_y,N'_y} g_{N'_y,N'_x} \Sigma^{(4)}_{N'_x,D_x}$. Assuming symmetric contacts yields $\Gamma_{D_x,N'_x,N'_x,D_x} = \Gamma_{D_y,N'_y,N'_y,D_y} \equiv \Gamma_{\rm loc}$ and $\Gamma_{D_x,N'_x,N'_y,D_y} = \Gamma_{D_y,N'_y,N'_x,D_x} \equiv \Gamma_{\rm nonloc}$. The energy levels are given by

$$\omega_{(\pm)} = \Gamma_{\rm loc} \pm \Gamma_{\rm nonloc} \tag{A4}$$

$$= \left(\Sigma^{(4)}\right)^2 [B_R \pm A_R] + i\left(\Sigma^{(4)}\right)^2 [B_I \pm A_I], \tag{A5}$$

where A_R, A_I, B_R, and B_I are given by Eqs. (58)–(61).

Now, we assume $B_R = B_I = 0$, as in Sec. V. Then, Eqs. (A4) and (A5) yield energy levels $\omega_{(\pm)} = \pm\Sigma^{(4)}(A_R + iA_I)$ having opposite real and imaginary parts.

APPENDIX B: $V = 0^+$ ADIABATIC LIMIT

In this Appendix, we examine the $V = 0^+$ adiabatic limit of four-terminal Josephson junctions containing a single or two quantum dots (see Appendixes B 1 and B 2 below).

1. Single quantum dot

We start with single 0D quantum dots in the $V = 0^+$ adiabatic limit, summarizing a fraction of the Supplemental Material of our previous Paper II [88].

The Dyson equations take the following form for the considered 0D quantum dot connected to p_0 superconducting leads by the tunnel amplitudes $\hat{\Sigma}^{(5)}_{D_x,S_{n_p}} = \hat{\Sigma}^{(5)}_{S_{n_p},D_x}$, with $n_p = 1, \ldots, p_0$:

$$\hat{G}_{D_x,D_x} = \hat{g}_{D_x,D_x} + \hat{g}_{D_x,D_x} \sum_{n_p=1}^{p_0} \hat{\Sigma}^{(5)}_{D_x,S_{n_p}} \hat{g}_{S_{n_p},S_{n_p}} \hat{\Sigma}^{(5)}_{S_{n_p},D_x} \hat{G}_{D_x,D_x}. \tag{B1}$$

In the infinite-gap limit, Eq. (B1) can be expressed with the infinite-gap Hamiltonian $\hat{\mathscr{H}}^{(\infty)}_{\rm eff,\,single\,dot}$:

$$\hat{G}^A_{D_x,D_x} = \left(\omega - i\eta - \hat{\mathscr{H}}^{(\infty)}_{\rm eff,\,single\,dot}\right)^{-1}, \tag{B2}$$

where

$$\hat{\mathscr{H}}^{(\infty)}_{\rm eff,\,single\,dot} = \sum_{n_p=1}^{p_0} \hat{\Sigma}^{(5)}_{D_x,S_{n_p}} \hat{g}_{S_{n_p},S_{n_p}} \hat{\Sigma}^{(5)}_{S_{n_p},D_x}. \tag{B3}$$

Specifically, we obtain the following with $p_0 = 4$ superconducting leads:

$$\hat{\mathscr{H}}^{(\infty)}_{\rm eff,\,single\,dot} = \begin{pmatrix} 0 & \gamma_{D_x,D_x} \\ (\gamma_{D_x,D_x})^* & 0 \end{pmatrix}, \tag{B4}$$

where

$$\gamma_{D_x,D_x} = \Gamma_a \exp(i\varphi_a) + \Gamma_b \exp(i\varphi_b) + \Gamma_{c,1} \exp(i\varphi_{c,1}) + \Gamma_{c,2} \exp(i\varphi_{c,2}), \tag{B5}$$

and $\Gamma_{n_p} = (\Sigma^{(5)}_{D_x,S_{n_p}})^2/W$ parametrizes the linewidth broadening of the quantum dot level in the normal state.

The $(S_{c,1}, S_{c,2})$ superconducting leads can be gathered into the single $S_{c,\rm eff}$ coupled by

$$\Gamma_{c,\rm eff} = \Gamma_{c,1} \exp(i\varphi_{c,1}) + \Gamma_{c,2} \exp(i\varphi_{c,2}). \tag{B6}$$

Using the identical $\Gamma_{c,1} = \Gamma_{c,2} \equiv \Gamma_c$ and the gauge given by Eqs. (2) and (3) yields

$$\Gamma_{c,\rm eff} = \Gamma_c [1 + \exp(i\Phi)] \exp(i\varphi_{c,1}). \tag{B7}$$

It was shown in the Supplemental Material of our previous Paper II [88] that nonsymmetric coupling to the superconducting leads can produce inversion between $\Phi = 0$ and π in the infinite-gap limit. But, Eq. (B7) implies $|\Gamma_{c,\rm eff}| = 2\Gamma_c$ if $\Phi = 0$ and $\Gamma_{c,\rm eff} = 0$ if $\Phi = \pi$ for symmetric couplings to the superconducting leads, i.e., the quartet current at $\Phi = \pi$ is vanishingly small, thus it is automatically smaller than at $\Phi = 0$.

2. Double 0D quantum dot

In this section, we provide a simple argument for emergence of inversion in the double 0D quantum dot with normal lead in parallel in Fig. 3, in the limits $eV/\Delta = 0^+$ and $\Gamma' = 0$. In the infinite-gap limit, the 4×4 Hamiltonian of a double 0D quantum dot with normal leads in parallel is given by

$$\hat{\mathscr{H}}^{(\infty)}_{\rm eff,\,double\,dot} = \begin{pmatrix} 0 & \gamma_{D_x,D_x} & \Sigma^{(0)} & 0 \\ (\gamma_{D_x,D_x})^* & 0 & 0 & -\Sigma^{(0)} \\ \Sigma^{(0)} & 0 & 0 & \gamma_{D_y,D_y} \\ 0 & -\Sigma^{(0)} & (\gamma_{D_y,D_y})^* & 0 \end{pmatrix}, \tag{B8}$$

where we assumed $\Gamma' = 0$, and γ_{D_x,D_x}, γ_{D_y,D_y} are given by Eqs. (84) and (85). Squaring the infinite-gap Hamiltonian given by Eq. (B8) leads to

$$\left(\hat{\mathscr{H}}^{(\infty)}_{\rm eff,\,double\,dot}\right)^2 \begin{pmatrix} |\gamma_{D_x,D_x}|^2 + (\Sigma^{(0)})^2 & 0 & 0 & -\Sigma^{(0)}[\gamma_{D_x,D_x} - \gamma_{D_y,D_y}] \\ 0 & |\gamma_{D_x,D_x}|^2 + (\Sigma^{(0)})^2 & \Sigma^{(0)}[(\gamma_{D_x,D_x})^* - (\gamma_{D_y,D_y})^*] & 0 \\ 0 & \Sigma^{(0)}[\gamma_{D_x,D_x} - \gamma_{D_y,D_y}] & |\gamma_{D_y,D_y}|^2 + (\Sigma^{(0)})^2 & 0 \\ -\Sigma^{(0)}[(\gamma_{D_x,D_x})^* - (\gamma_{D_y,D_y})^*] & 0 & 0 & |\gamma_{D_y,D_y}|^2 + (\Sigma^{(0)})^2 \end{pmatrix}, \tag{B9}$$

which decouples into the following 2×2 blocks:

$$[\hat{\mathscr{H}}^2]^{(0)}_{2\times 2} = \begin{pmatrix} |\gamma_{D_x,D_x}|^2 + \left(\Sigma^{(0)}\right)^2 & -\Sigma^{(0)}\left[\gamma_{D_x,D_x} - \gamma_{D_y,D_y}\right] \\ -\Sigma^{(0)}\left[\left(\gamma_{D_x,D_x}\right)^* - \left(\gamma_{D_y,D_y}\right)^*\right] & |\gamma_{D_y,D_y}|^2 + \left(\Sigma^{(0)}\right)^2 \end{pmatrix} \tag{B10}$$

and

$$[\hat{\mathscr{H}}^2]^{(2)}_{2\times 2} = \begin{pmatrix} |\gamma_{D_x,D_x}|^2 + \left(\Sigma^{(0)}\right)^2 & \Sigma^{(0)}\left[\left(\gamma_{D_x,D_x}\right)^* - \left(\gamma_{D_y,D_y}\right)^*\right] \\ \Sigma^{(0)}\left[\gamma_{D_x,D_x} - \gamma_{D_y,D_y}\right] & |\gamma_{D_y,D_y}|^2 + \left(\Sigma^{(0)}\right)^2 \end{pmatrix}. \tag{B11}$$

Thus,

$$\gamma_{D_x,D_x} - \gamma_{D_y,D_y} = \Gamma_a \exp(i\varphi_a) + \Gamma_{c,1} \exp(i\varphi_{c,1}) - \Gamma_b \exp(i\varphi_b) - \Gamma_{c,2} \exp(i\varphi_{c,2}) \tag{B12}$$

and the coupling to the effective $S_{c,\mathrm{eff}}$ is now given by the difference

$$\Gamma_{c,\mathrm{eff}} = \Gamma_{c,1} \exp(i\varphi_{c,1}) - \Gamma_{c,2} \exp(i\varphi_{c,2}) \tag{B13}$$

instead of the previous Eq. (B6) for a single 0D quantum dot. Equation (B13) goes to

$$\Gamma_{c,\mathrm{eff}}(\Phi) = \Gamma[1 - \exp(i\Phi)] \exp(i\varphi_{c,1}) \tag{B14}$$

in the considered limit $\Gamma_{c,1} = \Gamma_{c,2} \equiv \Gamma$ of symmetric couplings. Thus, the interference $|\Gamma_{c,\mathrm{eff}}|(\Phi = 0) = 0$ and $|\Gamma_{c,\mathrm{eff}}|(\Phi = \pi) = 2\Gamma$ yields inversion between $\Phi = 0$ and π with symmetric coupling to the superconducting leads. This contrasts with absence of inversion for single 0D quantum dots (see Appendix B 1).

[1] J. Bardeen, L. N. Cooper, and J. R. Schrieffer, Theory of superconductivity, Phys. Rev. **108**, 1175 (1957).

[2] P. W. Anderson, Random-phase approximation in the theory of superconductivity, Phys. Rev. **112**, 1900 (1958).

[3] P. W. Anderson, Plasmons, gauge invariance, and mass, Phys. Rev. **130**, 439 (1963).

[4] B. D. Josephson, Possible new effects in superconductive tunnelling, Phys. Lett. **1**, 251 (1962).

[5] A. F. Andreev, Thermal conductivity of the intermediate state of superconductors, Sov. Phys.–JETP **20**, 1490 (1965) [J. Exp. Theor. Phys. **47**, 2222 (1964)].

[6] P. G. de Gennes and D. Saint-James, Elementary excitations in the vicinity of a normal metal-superconducting metal contact, Phys. Lett. **4**, 151 (1963).

[7] D. Saint-James, Excitations élémentaires au voisinage de la surface de séparation d'un métal normal et d'un métal supraconducteur, J. Phys. (France) **25**, 899 (1964).

[8] I. O. Kulik, Macroscopic quantization and the proximity effect in SNS junctions, Zh. Eksp. Teor. Fiz. **57**, 1745 (1969) [Sov. Phys.–JETP **30**, 944 (1970)].

[9] K. K. Likharev, Superconducting weak links, Rev. Mod. Phys. **51**, 101 (1979).

[10] D. Averin and H. T. Imam, Supercurrent Noise in Quantum Point Contacts, Phys. Rev. Lett. **76**, 3814 (1996).

[11] J. C. Cuevas, A. Martín-Rodero, and A. Levy Yeyati, Hamiltonian approach to the transport properties of superconducting quantum point contacts, Phys. Rev. B **54**, 7366 (1996).

[12] E. Scheer, N. Agraït, J. C. Cuevas, A. Levy Yeyati, B. Ludophk, A. Martín-Rodero, G. Rubio Bollinger, J. M. van Ruitenbeekk, and C. Urbina, The signature of chemical valence in the electrical conduction through a single-atom contact, Nature (London) **394**, 154 (1998).

[13] C. W. Beenakker, in *Proceedings of the 14th Taniguchi International Symposium on Transport Phenomena in Mesoscopic Systems*, edited by H. Fukuyama and T. Ando (Springer, Berlin, 1992).

[14] L. Bretheau, Ç. Ö. Girit, D. Esteve, H. Pothier, and C. Urbina, Tunnelling spectroscopy of Andreev states in graphene, Nature (London) **499**, 312 (2013).

[15] L. Bretheau, Ç. Ö. Girit, C. Urbina, D. Esteve, and H. Pothier, Supercurrent Spectroscopy of Andreev States, Phys. Rev. X **3**, 041034 (2013).

[16] D. G. Olivares, A. L. Yeyati, L. Bretheau, Ç. Ö. Girit, H. Pothier, and C. Urbina, Dynamics of quasiparticle trapping in Andreev levels, Phys. Rev. B **89**, 104504 (2014).

[17] C. Janvier, L. Tosi, L. Bretheau, Ç. Ö. Girit, M. Stern, P. Bertet, P. Joyez, D. Vion, D. Esteve, M. F. Goffman, H. Pothier, and C. Urbina, Coherent manipulation of Andreev states in superconducting atomic contacts, Science **349**, 1199 (2015).

[18] A. Zazunov, V. S. Shumeiko, E. N. Bratus', J. Lantz, and G. Wendin, Andreev Level Qubit, Phys. Rev. Lett. **90**, 087003 (2003).

[19] J. M. Martinis, M. Ansmann, and J. Aumentado, Energy Decay in Superconducting Josephson-Junction Qubits from Nonequilibrium Quasiparticle Excitations, Phys. Rev. Lett. **103**, 097002 (2009).

[20] P. J. de Visser, J. J. A. Baselmans, P. Diener, S. J. C. Yates, A. Endo, and T. M. Klapwijk, Number Fluctuations of Sparse Quasiparticles in a Superconductor, Phys. Rev. Lett. **106**, 167004 (2011).

[21] M. Lenander, H. Wang, R. C. Bialczak, E. Lucero, M. Mariantoni, M. Neeley, A. D. O'Connell, D. Sank, M. Weides, J. Wenner, T. Yamamoto, Y. Yin, J. Zhao, A. N. Cleland, and J. M. Martinis, Measurement of energy decay in

superconducting qubits from nonequilibrium quasiparticles, Phys. Rev. B **84**, 024501 (2011).

[22] S. Rajauria, L. M. A. Pascal, Ph. Gandit, F. W. J. Hekking, B. Pannetier, and H. Courtois, Efficiency of quasiparticle evacuation in superconducting devices, Phys. Rev. B **85**, 020505(R) (2012).

[23] J. Wenner, Y. Yin, E. Lucero, R. Barends, Y. Chen, B. Chiaro, J. Kelly, M. Lenander, M. Mariantoni, A. Megrant, C. Neill, P. J. J. O'Malley, D. Sank, A. Vainsencher, H. Wang, T. C. White, A. N. Cleland, and J. M. Martinis, Excitation of Superconducting Qubits from Hot Nonequilibrium Quasiparticles, Phys. Rev. Lett. **110**, 150502 (2013).

[24] D. Ristè, C. C. Bultink, M. J. Tiggelman, R. N. Schouten, K. W. Lehnert, and L. DiCarlo, Millisecond charge-parity fluctuations and induced decoherence in a superconducting transmon qubit, Nat. Commun. **4**, 1913 (2013).

[25] E. M. Levenson-Falk, F. Kos, R. Vijay, L. Glazman, and I. Siddiqi, Single-Quasiparticle Trapping in Aluminum Nanobridge Josephson Junctions, Phys. Rev. Lett. **112**, 047002 (2014).

[26] J. S. Meyer, M. Houzet, and A. V. Nazarov, Dynamical Spin Polarization of Excess Quasiparticles in Superconductors, Phys. Rev. Lett. **125**, 097006 (2020).

[27] D. Kouznetsov, D. Rohrlich, and R. Ortega, Quantum limit of noise of a phase-invariant amplifier, Phys. Rev. A **52**, 1665 (1995).

[28] *The SQUID Handbook Vol. I Fundamentals and Technology of SQUIDs and SQUID Systems*, edited by J. Clarke, and A. I. Braginski (Wiley-Vch, Weinheim, 2004).

[29] J. Clarke and F. K. Wilhelm, Superconducting quantum bits, Nature (London) **453**, 1031 (2008).

[30] M. H. Devoret and R. J. Schoelkopf, Superconducting circuits for quantum information: An outlook, Science **339**, 1169 (2013).

[31] F. Arute *et al.*, Quantum supremacy using a programmable superconducting processor, Nature (London) **574**, 505 (2019).

[32] S. B. Kaplan, C. C. Chi, D. N. Langenberg, J. J. Chang, S. Jafarey, and D. J. Scalapino, Quasiparticle and phonon lifetimes in superconductors, Phys. Rev. B **14**, 4854 (1976).

[33] R. C. Dynes, V. Narayanamurti, and J. P. Garno, Direct Measurement of Quasiparticle-Lifetime Broadening in a Strong-Coupled Superconductor, Phys. Rev. Lett. **41**, 1509 (1978).

[34] J. P. Pekola, V. F. Maisi, S. Kafanov, N. Chekurov, A. Kemppinen, Yu. A. Pashkin, O.-P. Saira, M. Möttönen, and J. S. Tsai, Environment-Assisted Tunneling as an Origin of the Dynes Density of States, Phys. Rev. Lett. **105**, 026803 (2010).

[35] O.-P. Saira, A. Kemppinen, V. F. Maisi, and J. P. Pekola, Vanishing quasiparticle density in a hybrid Al/Cu/Al single-electron transistor, Phys. Rev. B **85**, 012504 (2012).

[36] T. Meng, S. Florens, and P. Simon, Self-consistent description of Andreev bound states in Josephson quantum dot devices, Phys. Rev. B **79**, 224521 (2009).

[37] R. L. Klees, G. Rastelli, J. C. Cuevas, and W. Belzig, Microwave Spectroscopy Reveals the Quantum Geometric Tensor of Topological Josephson Matter, Phys. Rev. Lett. **124**, 197002 (2020).

[38] N. K. Allsopp, V. C. Hui, C. J. Lambert, and S. J. Robinson, Theory of the sign of multi-probe conductances for normal and superconducting materials, J. Phys.: Condens. Matter **6**, 10475 (1994).

[39] J. M. Byers and M. E. Flatté, Probing Spatial Correlations with Nanoscale Two-Contact Tunneling, Phys. Rev. Lett. **74**, 306 (1995).

[40] J. Torrès and T. Martin, Positive and negative Hanbury-Brown and Twiss correlations in normal metal-superconducting devices, Eur. Phys. J. B **12**, 319 (1999).

[41] G. Deutscher and D. Feinberg, Coupling superconducting-ferromagnetic point contacts by Andreev reflections, Appl. Phys. Lett. **76**, 487 (2000).

[42] M. S. Choi, C. Bruder, and D. Loss, Spin-dependent Josephson current through double quantum dots and measurement of entangled electron states, Phys. Rev. B **62**, 13569 (2000).

[43] G. Falci, D. Feinberg, and F. W. J. Hekking, Correlated tunneling into a superconductor in a multiprobe hybrid structure, Europhys. Lett. **54**, 255 (2001).

[44] P. Recher, E. V. Sukhorukov, and D. Loss, Andreev tunneling, Coulomb blockade, and resonant transport of nonlocal spin-entangled electrons, Phys. Rev. B **63**, 165314 (2001).

[45] G. B. Lesovik, T. Martin, and G. Blatter, Electronic entanglement in the vicinity of a superconductor, Eur. Phys. J. B **24**, 287 (2001).

[46] R. Mélin and D. Feinberg, Transport theory of multiterminal hybrid structures, Eur. Phys. J. B **26**, 101 (2002).

[47] N. M. Chtchelkatchev, G. Blatter, G. B. Lesovik, and T. Martin, Bell inequalities and entanglement in solid-state devices, Phys. Rev. B **66**, 161320(R) (2002).

[48] R. Mélin and D. Feinberg, Sign of the crossed conductances at a ferromagnet/superconductor/ferromagnet double interface, Phys. Rev. B **70**, 174509 (2004).

[49] A. V. Lebedev, G. B. Lesovik, and G. Blatter, Generating spin-entangled electron pairs in normal conductors using voltage pulses, Phys. Rev. B **72**, 245314 (2005).

[50] K. V. Bayandin, G. B. Lesovik, and T. Martin, Energy entanglement in normal metal-superconducting forks, Phys. Rev. B **74**, 085326 (2006).

[51] A. L. Yeyati, F. S. Bergeret, A. Martín-Rodero, and T. M. Klapwijk, Entangled Andreev pairs and collective excitations in nanoscale superconductors, Nat. Phys. **3**, 455 (2007).

[52] D. Beckmann, H. B. Weber, and H. v. Löhneysen, Evidence for Crossed Andreev Reflection in Superconductor-Ferromagnet Hybrid Structures, Phys. Rev. Lett. **93**, 197003 (2004).

[53] S. Russo, M. Kroug, T. M. Klapwijk, and A. F. Morpurgo, Experimental Observation of Bias-Dependent Nonlocal Andreev Reflection, Phys. Rev. Lett. **95**, 027002 (2005).

[54] P. Cadden-Zimansky and V. Chandrasekhar, Nonlocal Correlations in Normal-Metal Superconducting Systems, Phys. Rev. Lett. **97**, 237003 (2006).

[55] D. Beckmann, H. B. Weber, and H. v. Löhneysen, Negative four-terminal resistance as a probe of crossed Andreev reflection, Appl. Phys. A **89**, 603 (2007).

[56] P. Cadden-Zimansky, Z. Jiang, and V. Chandrasekhar, Charge imbalance, crossed Andreev reflection and elastic co-tunnelling in ferromagnet/superconductor/normal-metal structures, New J. Phys. **9**, 116 (2007).

[57] L. Hofstetter, S. Csonka, J. Nygard, and C. Schönenberger, Cooper pair splitter realized in a two-quantum-dot Y-junction, Nature (London) **461**, 960 (2009).

[58] L. G. Herrmann, F. Portier, P. Roche, A. Levy Yeyati, T. Kontos, and C. Strunk, Carbon Nanotubes as Cooper-Pair Beam Splitters, Phys. Rev. Lett. **104**, 026801 (2010).
[59] J. Wei and V. Chandrasekhar, Positive noise cross-correlation in hybrid superconducting and normal-metal three-terminal devices, Nat. Phys. **6**, 494 (2010).
[60] A. Das, Y. Ronen, M. Heiblum, D. Mahalu, A. V. Kretinin, and H. Shtrikman, High-efficiency Cooper pair splitting demonstrated by two-particle conductance resonance and positive noise cross- correlation, Nat. Commun. **3**, 1165 (2012).
[61] J. Schindele, A. Baumgartner, and C. Schönenberger, Near-Unity Cooper Pair Splitting Efficiency, Phys. Rev. Lett. **109**, 157002 (2012).
[62] J. Schindele, A. Baumgartner, R. Maurand, M. Weiss, and C. Schönenberger, Nonlocal spectroscopy of Andreev bound states, Phys. Rev. B **89**, 045422 (2014).
[63] Z. B. Tan, D. Cox, T. Nieminen, P. Lähteenmäki, D. Golubev, G. B. Lesovik, and P. J. Hakonen, Cooper Pair Splitting by Means of Graphene Quantum Dots, Phys. Rev. Lett. **114**, 096602 (2015).
[64] I. V. Borzenets, Y. Shimazaki, G. F. Jones, M. F. Craciun, S. Russo, M. Yamamoto, and S. Tarucha, High Efficiency CVD Graphene-lead (Pb) Cooper Pair Splitter, Sci. Rep. **6**, 23051 (2016).
[65] P. Pandey, R. Danneau, and D. Beckmann, Ballistic Graphene Cooper Pair Splitter, Phys. Rev. Lett. **126**, 147701 (2021).
[66] M. P. Anantram and S. Datta, Current fluctuations in mesoscopic systems with Andreev scattering, Phys. Rev. B **53**, 16390 (1996).
[67] P. Samuelsson and M. Büttiker, Chaotic Dot-Superconductor Analog of the Hanbury Brown–Twiss Effect, Phys. Rev. Lett. **89**, 046601 (2002).
[68] P. Samuelsson and M. Büttiker, Semiclassical theory of current correlations in chaotic dot-superconductor systems, Phys. Rev. B **66**, 201306(R) (2002).
[69] J. Börlin, W. Belzig, and C. Bruder, Full Counting Statistics of a Superconducting Beam Splitter, Phys. Rev. Lett. **88**, 197001 (2002).
[70] P. Samuelsson, E. V. Sukhorukov, and M. Büttiker, Orbital Entanglement and Violation of Bell Inequalities in Mesoscopic Conductors, Phys. Rev. Lett. **91**, 157002 (2003).
[71] L. Faoro, F. Taddei, and R. Fazio, Clauser-Horne inequality for electron-counting statistics in multiterminal mesoscopic conductors, Phys. Rev. B **69**, 125326 (2004).
[72] G. Bignon, M. Houzet, F. Pistolesi, and F. W. J. Hekking, Current-current correlations in hybrid superconducting and normal metal multiterminal structures, Europhys. Lett. **67**, 110 (2004).
[73] R. Mélin, C. Benjamin, and T. Martin, Positive cross correlations of noise in superconducting hybrid structures: Roles of interfaces and interactions, Phys. Rev. B **77**, 094512 (2008).
[74] A. Freyn, M. Flöser, and R. Mélin, Positive current cross-correlations in a highly transparent normal-superconducting beam splitter due to synchronized Andreev and inverse Andreev reflections, Phys. Rev. B **82**, 014510 (2010).
[75] D. S. Golubev and A. D. Zaikin, Shot noise and Coulomb effects on nonlocal electron transport in normal-metal/superconductor/normal-metal heterostructures, Phys. Rev. B **82**, 134508 (2010).
[76] M. Flöser, D. Feinberg, and R. Mélin, Absence of split pairs in cross correlations of a highly transparent normal metal-superconductor-normal metal electron-beam splitter, Phys. Rev. B **88**, 094517 (2013).
[77] G. Michałek, B. R. Bulka, T. Domański, and K. I. Wysokiński, Statistical correlations of currents flowing through a proximitized quantum dot, Phys. Rev. B **101**, 235402 (2020).
[78] J. C. Cuevas and H. Pothier, Voltage-induced Shapiro steps in a superconducting multiterminal structure, Phys. Rev. B **75**, 174513 (2007).
[79] A. Freyn, B. Douçot, D. Feinberg, and R. Mélin, Production of Nonlocal Quartets and Phase-Sensitive Entanglement in a Superconducting Beam Splitter, Phys. Rev. Lett. **106**, 257005 (2011).
[80] T. Jonckheere, J. Rech, T. Martin, B. Douçot, D. Feinberg, and R. Mélin, Multipair DC Josephson resonances in a biased all-superconducting bijunction, Phys. Rev. B **87**, 214501 (2013).
[81] R. Mélin, D. Feinberg, and B. Douçot, Partially resummed perturbation theory for multiple Andreev reflections in a short three-terminal Josephson junction, Eur. Phys. J. B **89**, 67 (2016).
[82] R. Mélin, M. Sotto, D. Feinberg, J.-G. Caputo, and B. Douçot, Gate-tunable zero-frequency current cross-correlations of the quartet mode in a voltage-biased three-terminal Josephson junction, Phys. Rev. B **93**, 115436 (2016).
[83] R. Mélin, J.-G. Caputo, K. Yang, and B. Douçot, Simple Floquet-Wannier-Stark-Andreev viewpoint and emergence of low-energy scales in a voltage-biased three-terminal Josephson junction, Phys. Rev. B **95**, 085415 (2017).
[84] R. Mélin, R. Danneau, K. Yang, J.-G. Caputo, and B. Douçot, Engineering the Floquet spectrum of superconducting multiterminal quantum dots, Phys. Rev. B **100**, 035450 (2019).
[85] J. D. Pillet, V. Benzoni, J. Griesmar, J.-L. Smirr, and Ç.Ö. Girit, Nonlocal Josephson Effect in Andreev Molecules Nano Lett. **19**, 7138 (2019).
[86] V. Kornich, H. S. Barakov, and Yu. V. Nazarov, Fine energy splitting of overlapping Andreev bound states in multiterminal superconducting nanostructures, Phys. Rev. Research **1**, 033004 (2019).
[87] R. Mélin, Inversion in a four terminal superconducting device on the quartet line. I. Two-dimensional metal and the quartet beam splitter, Phys. Rev. B **102**, 245435 (2020).
[88] R. Mélin and B. Douçot, Inversion in a four terminal superconducting device on the quartet line. II. Quantum dot and Floquet theory, Phys. Rev. B **102**, 245436 (2020).
[89] J.-D. Pillet, V. Benzoni, J. Griesmar, J.-L. Smirr, and Ç. Ö. Girit, Scattering description of Andreev molecules, SciPost Phys. Core **2**, 009 (2020).
[90] V. Kornich, H. S. Barakov, and Yu. V. Nazarov, Overlapping Andreev states in semiconducting nanowires: Competition of 1D and 3D propagation, Phys. Rev. B **101**, 195430 (2020).
[91] R. Mélin, Ultralong-distance quantum correlations in three-terminal Josephson junctions, Phys. Rev. B **104**, 075402 (2021).
[92] A. Melo, V. Fatemi, and A. R. Akhmerov, Multiplet supercurrent in Josephson tunneling circuits, SciPost Phys. **12**, 017 (2022).

[93] A. H. Pfeffer, J. E. Duvauchelle, H. Courtois, R. Mélin, D. Feinberg, and F. Lefloch, Subgap structure in the conductance of a three-terminal Josephson junction, Phys. Rev. B **90**, 075401 (2014).

[94] E. Strambini, S. D'Ambrosio, F. Vischi, F. S. Bergeret, Yu. V. Nazarov, and F. Giazotto, The ω-SQUIPT as a tool to phase-engineer Josephson topological materials, Nat. Nanotechnol. **11**, 1055 (2016).

[95] Y. Cohen, Y. Ronen, J. H. Kang, M. Heiblum, D. Feinberg, R. Mélin, and H. Strikman, Non-local supercurrent of quartets in a three-terminal Josephson junction, Proc. Natl. Acad. Sci. U.S.A. **115**, 6991 (2018).

[96] A. W. Draelos, M.-T. Wei, A. Seredinski, H. Li, Y. Mehta, K. Watanabe, T. Taniguchi, I. V. Borzenets, F. Amet, and G. Finkelstein, Supercurrent flow in multiterminal graphene Josephson junctions, Nano Lett. **19**, 1039 (2019).

[97] K. F. Huang, Y. Ronen, R. Mélin, D. Feinberg, K. Watanabe, T. Taniguchi, and P. Kim, Quartet supercurrent in a multi-terminal Graphene-based Josephson Junction, arXiv:2008.03419.

[98] N. Pankratova, H. Lee, R. Kuzmin, K. Wickramasinghe, W. Mayer, J. Yuan, M. Vavilov, J. Shabani, and V. Manucharyan, Multiterminal Josephson Effect, Phys. Rev. X **10**, 031051 (2020).

[99] G. V. Graziano, J. S. Lee, M. Pendharkar, C. Palmstrom, and V. S. Pribiag, Transport studies in a gate-tunable three-terminal Josephson junction, Phys. Rev. B **101**, 054510 (2020).

[100] E. G. Arnault, T. Larson, A. Seredinski, L. Zhao, H. Li, K. Watanabe, T. Tanniguchi, I. Borzenets, F. Amet, and G. Finkelstein, The multiterminal inverse AC Josephson effect, arXiv:2012.15253.

[101] S. A. Khan, L. Stampfer, T. Mutas, J.-H. Kang, P. Krogstrup, and T. S. Jespersen, Multiterminal quantized conductance in InSb nanocrosses, arXiv:2101.02529.

[102] O. Kürtössy, Z. Scherübl, G. Fülöp, I. E. Lukács, T. Kanne, J. Nygard, P. Makk, and S. Csonka, Andreev molecule in parallel InAs nanowires, arXiv:2103.14083.

[103] G. V. Graziano, M. Gupta, M. Pendharkar, J. T. Dong, C. P. Dempsey, C. Palmstrom, and V. S. Pribiag, Selective Control of Conductance Modes in Multi-terminal Josephson Junctions, arXiv:2201.01373.

[104] E. G. Arnault, S. Idris, A. McConnell, L. Zhao, T. F. Q. Larson, K. Watanabe, T. Taniguchi, G. Finkelstein, and F. Amet, Dynamical stabilization of multiplet supercurrents in multi-terminal Josephson junctions, arXiv:2201.11180.

[105] B. van Heck, S. Mi, and A. R. Akhmerov, Single fermion manipulation via superconducting phase differences in multiterminal Josephson junctions, Phys. Rev. B **90**, 155450 (2014).

[106] C. Padurariu, T. Jonckheere, J. Rech, R. Mélin, D. Feinberg, T. Martin, and Yu. V. Nazarov, Closing the proximity gap in a metallic Josephson junction between three superconductors, Phys. Rev. B **92**, 205409 (2015).

[107] R.-P. Riwar, M. Houzet, J. S. Meyer, and Y. V. Nazarov, Multi-terminal Josephson junctions as topological materials, Nat. Commun. **7**, 11167 (2016).

[108] E. Eriksson, R.-P. Riwar, M. Houzet, J. S. Meyer, and Y. V. Nazarov, Topological transconductance quantization in a four-terminal Josephson junction, Phys. Rev. B **95**, 075417 (2017).

[109] O. Deb, K. Sengupta, and D. Sen, Josephson junctions of multiple superconducting wires, Phys. Rev. B **97**, 174518 (2018).

[110] V. Fatemi, A. R. Akhmerov, and L. Bretheau, Weyl Josepshon circuits, Phys. Rev. Research **3**, 013288 (2021).

[111] L. Peyruchat, J. Griesmar, J.-D. Pillet, and Ç.Ö. Girit, Transconductance quantization in a topological Josephson tunnel junction circuit, Phys. Rev. Research **3**, 013289 (2021).

[112] H. Weisbrich, R. L. Klees, G. Rastelli, and W. Belzig, Second Chern Number and Non-Abelian Berry Phase in Topological Superconducting Systems, PRX Quantum **2**, 010310 (2021).

[113] Y. Chen and Y. V. Nazarov, Weyl point immersed in a continuous spectrum: an example from superconducting nanostructures, Phys. Rev. B **104**, 104506 (2021).

[114] Y. Chen and Y. V. Nazarov, Spin-Weyl quantum unit: Theoretical proposal, Phys. Rev. B **103**, 045410 (2021).

[115] E. V. Repin and Y. V. Nazarov, Weyl points in the multiterminal hybrid superconductor-semiconductor nanowire devices, Phys. Rev. B **105**, L041405 (2022).

[116] B. Douçot, R. Danneau, K. Yang, J.-G. Caputo, and R. Mélin, Berry phase in superconducting multiterminal quantum dots, Phys. Rev. B **101**, 035411 (2020).

[117] B. Venitucci, D. Feinberg, R. Mélin, and B. Douçot, Nonadiabatic Josephson current pumping by microwave irradiation, Phys. Rev. B **97**, 195423 (2018).

[118] L. P. Gavensky, G. Usaj, D. Feinberg, and C. A. Balseiro, Berry curvature tomography and realization of topological Haldane model in driven three-terminal Josephson junctions, Phys. Rev. B **97**, 220505(R) (2018).

[119] H.-Y. Xie, M. G. Vavilov, and A. Levchenko, Topological Andreev bands in three-terminal Josephson junctions, Phys. Rev. B **96**, 161406(R) (2017).

[120] H.-Y. Xie, M. G. Vavilov, and A. Levchenko, Weyl nodes in Andreev spectra of multiterminal Josephson junctions: Chern numbers, conductances and supercurrents, Phys. Rev. B **97**, 035443 (2018).

[121] S. Park, W. Lee, S. Jang, Y.-B. Choi, J. Park, W. Jung, K. Watanabe, T. Taniguchi, G. Y. Cho, and G.-H. Lee, Steady Floquet-Andreev states in graphene Josephson junctions, Nature (London) **603**, 421 (2022).

[122] F. S. Bergeret, P. Virtanen, A. Ozaeta, T. T. Heikkilä, and J. C. Cuevas, Supercurrent and Andreev bound state dynamics in superconducting quantum point contacts under microwave irradiation, Phys. Rev. B **84**, 054504 (2011).

[123] A. Martín-Rodero, A. Levy Yeyati, and F. J. García-Vidal, Thermal noise in superconducting quantum point contacts, Phys. Rev. B **53**, R8891 (1996).

[124] C. Caroli, R. Combescot, P. Nozières, and D. Saint-James, Direct calculation of the tunneling current, J. Phys. C: Solid State Phys. **4**, 916 (1971).

[125] Yu. V. Nazarov and Y. M. Blanter, *Quantum Transport* (Cambridge University Press, Cambridge, 2012).

[126] C. Padurariu, T. Jonckheere, J. Rech, T. Martin, and D. Feinberg, Tunable pseudogaps due to nonlocal coherent transport in voltage-biased three-terminal Josephson junctions, Phys. Rev. B **95**, 205437 (2017).

[127] J.-D. Pillet, C. Quay, P. Morfin, C. Bena, A. Levy Yeyati, and P. Joyez, Revealing the electronic structure of a carbon nanotube carrying a supercurrent, Nat. Phys. **6**, 965 (2010).

[128] L. Bretheau, J. I.-J. Wang, R. Pisoni, K. Watanabe, T. Taniguchi, and P. Jarillo-Herrero, Tunnelling spectroscopy of Andreev states in graphene, Nat. Phys. **13**, 756 (2017).

[129] J. C. Cuevas, J. Hammer, J. Kopu, J. K. Viljas, and M. Eschrig, Proximity effect and multiple Andreev reflections in diffusive superconductor-normal-metal-superconductor junctions, Phys. Rev. B **73**, 184505 (2006).

[130] M. Vanević and W. Belzig, Full counting statistics of Andreev scattering in an asymmetric chaotic cavity, Phys. Rev. B **72**, 134522 (2005).

[131] G. E. Blonder, M. Tinkham, and T. M. Klapwijk, Transition from metallic to tunneling regimes in superconducting microconstrictions: Excess current, charge imbalance, and supercurrent conversion, Phys. Rev. B **25**, 4515 (1982).